

RESEARCH ARTICLE

The yeast LYST homolog Bph1 is a Rab5 effector and prevents Atg8 lipidation at endosomes

Prado Vargas Duarte¹, Ralph Hardenberg², Muriel Mari², Stefan Walter³, Fulvio Reggiori², Florian Fröhlich^{3,4}, Ayelén González Montoro^{3,5,*} and Christian Ungermann^{1,3,*}

ABSTRACT

Lysosomes mediate degradation of macromolecules to their precursors for cellular recycling. Additionally, lysosome-related organelles mediate cell type-specific functions. Chédiak–Higashi syndrome is an autosomal, recessive disease, in which loss of the protein LYST causes defects in lysosomes and lysosome-related organelles. The molecular function of LYST, however, is largely unknown. Here, we dissected the function of the yeast LYST homolog, Bph1. We show that Bph1 is an endosomal protein and an effector of the minor Rab5 isoform Ypt52. Strikingly, *bph1Δ* mutant cells have lipidated Atg8 on their endosomes, which is sorted via late endosomes into the vacuole lumen under non-autophagy-inducing conditions. In agreement with this, proteomic analysis of *bph1Δ* vacuoles reveals an accumulation of Atg8, reduced flux via selective autophagy, and defective endocytosis. Additionally, *bph1Δ* cells have reduced autophagic flux under starvation conditions. Our observations suggest that Bph1 is a novel Rab5 effector that maintains endosomal functioning. When Bph1 is lost, Atg8 is lipidated at endosomes even during normal growth and ends up in the vacuole lumen. Thus, our results contribute to the understanding of the role of LYST-related proteins and associated diseases.

KEY WORDS: Endosome, LYST, Rab5, Ypt52, Atg8, Autophagy, Endocytosis, Bph1

INTRODUCTION

The endolysosomal system functions in quality control of the plasma membrane by directing membrane proteins to the lysosome as the terminal lytic organelle. Endocytosis allows the internalization of plasma membrane proteins, which throughout the endosomal sorting pathway can be recycled back to the plasma membrane or sorted into intraluminal vesicles. Upon fusion with lysosomes, the intraluminal vesicles present in the late endosomes (LEs) are hydrolyzed, and the resulting molecules are exported into the cytoplasm for reuse. This pathway is conserved from simple

eukaryotes to mammalian neurons (Huotari and Helenius, 2011; Ferguson, 2018; Langemeyer et al., 2018; Wandinger-Ness and Zerial, 2014). The yeast *Saccharomyces cerevisiae* (hereafter yeast) has been a key model system for identification and characterization of the function of many conserved proteins and protein complexes in the endolysosomal system (Wada et al., 1992; Raymond et al., 1992; Robinson et al., 1988; Rothman and Stevens, 1986; Preston et al., 1992; Munn and Riezman, 1994).


Rab GTPases function as molecular signposts on organelles (Barr, 2013; Wandinger-Ness and Zerial, 2014; Hutagalung and Novick, 2011). They are present as soluble proteins in complex with their GDP dissociation inhibitor (GDI) chaperone, and they are recruited to membranes by an organelle-specific guanine-nucleotide-exchange factor (GEF), which exchanges the bound GDP with GTP. This GTP-bound form, which is anchored into the membranes of organelles, binds effector proteins. Rab proteins are inactivated with the help of a GTPase-activating protein, and the Rab is then extracted by the GDI chaperones. Due to this cycle, Rab GTPases spatially and temporally mark organelles with a specific set of proteins. Release of Rab GTPases also triggers dissociation of the effectors (Day et al., 2018). The endolysosomal system is characterized by Rab5 and Rab7 GTPases. Yeast harbors four Rab5-like proteins (Vps21, Ypt52, Ypt53 and Ypt10) and one Rab7 ortholog (Ypt7), which coordinate the transport and the functions of the endolysosomal system (Wichmann et al., 1992; Singer-Krüger et al., 1994; Horazdovsky et al., 1994).

Autophagy is a versatile and inducible catabolic pathway in which selected portions of the cytoplasm, organelles and/or pathogens are sequestered by growing disk-like structures, the phagophores, that upon closure form double-membrane vesicles, the autophagosomes (Zhao and Zhang, 2018; Nakatogawa, 2020). This process depends on multiple autophagy-related (ATG) genes and includes the conjugation of the ubiquitin-like Atg8 protein to phosphatidylethanolamine (PE) on the surface of autophagosomes (Zhao and Zhang, 2018; Nakatogawa, 2020). During their formation and maturation, autophagosomes acquire the machinery to fuse with lysosomes (Zhao and Zhang, 2018; Reggiori and Ungermann, 2017). Lysosomal hydrolases then degrade the luminal content of the autophagosomes. It is thus not surprising that lysosomes harbor nutrient-sensing complexes such as the target of rapamycin complex 1 (TORC1), whose signaling controls numerous catabolic processes, including autophagy, and anabolic ones, like cell growth (Shin and Zoncu, 2020; Virgilio, 2012; Saxton and Sabatini, 2017).

Lysosome-related organelles (LROs) are a branch of the endolysosomal system in selected cell types, in which a subpopulation of lysosomes acquires a specific function due to a distinct protein repertoire (Bowman et al., 2019). Well-known examples are melanosomes and Weibel–Palade bodies, although the list of LROs goes far beyond these (Bowman et al., 2019). Owing to their special function, mutations in proteins involved in LRO

¹Osnabrück University, Department of Biology/Chemistry, Biochemistry section, Barbarastrasse 13, 49076 Osnabrück, Germany. ²Department of Biomedical Sciences of Cells and Systems, University of Groningen, University Medical Center Groningen, 9700 Groningen, The Netherlands. ³Osnabrück University, Center of Cellular Nanoanalytic Osnabrück (CellNanOs), Barbarastrasse 11, 49076 Osnabrück, Germany. ⁴Osnabrück University, Department of Biology/Chemistry, Molecular Membrane Biology section, Barbarastrasse 13, 49076 Osnabrück, Germany. ⁵Osnabrück University, Department of Biology/Chemistry, Cellular Communication Laboratory, Barbarastrasse 13, 49076 Osnabrück, Germany.

*Authors for correspondence (ayelen.gonzalez.montoro@uos.de; cu@uos.de)

 F.R., 0000-0003-2652-2686; A.G.M., 0000-0002-6978-8284; C.U., 0000-0003-4331-8695

Handling Editor: Jennifer Lippincott-Schwartz
Received 30 September 2021; Accepted 18 March 2022

biogenesis can have severe pathological consequences, but they do not impair the overall development of the organism in most cases. One of the human diseases caused by an impairment in LRO biogenesis is Chédiak–Higashi syndrome, a rare autosomal disease (Perou et al., 1997; Sharma et al., 2019). This disease is caused by the loss of lysosomal-trafficking regulator (LYST), a large 430 kDa protein with a C-terminal BEACH (Beige and Chédiak–Higashi) domain followed by a β -propeller domain. Whereas β -propeller domains are known to mediate multiple types of interactions, including binding to phosphoinositides and other proteins (Dove et al., 2004; Gomez-Navarro and Miller, 2016), the function of the BEACH domain remains unclear (Cullinane et al., 2013; Teh et al., 2015). Insights into LYST function stem primarily from knockout analyses, both in cells containing LROs and standard cells (Faigle et al., 1998; Charette and Cosson, 2007; Rahman et al., 2012; Cullinane et al., 2013; Holland et al., 2014; Falkenstein and Lozanne, 2014; Sepulveda et al., 2015). Loss of LYST or homologous proteins results in enlarged lysosomes, which suggests a function in membrane fusion or fission (Holland et al., 2014; Falkenstein and Lozanne, 2014; Sepulveda et al., 2015). However, due to the size of the protein and the lack of suitable assays, LYST molecular function at endosomes and/or lysosomes remains unknown.

Yeast has just one BEACH-domain-containing protein, Bph1. Bph1 has the same domain organization as LYST, with a C-terminal BEACH domain followed by a putative β -propeller domain (Shiflett et al., 2004) (Fig. 1A). Bph1 localizes partially to membranes, and its deletion has mild effects on both growth on the cell wall chelator Calcofluor White and selective autophagy of a stalled endocytic compartments, suggesting a role for Bph1 in the endocytic pathway (Shiflett et al., 2004; Wilfling et al., 2020). Insights into Bph1 molecular function, however, are lacking. Here, we show that Bph1 is an endosomal protein and effector of Ypt52, one of the yeast Rab5 isoforms. Bph1 is required for endosomal function and is linked to autophagy. In particular, cells lacking *BPH1* have a defined defect in endocytosis, as revealed by vacuolar proteomics and assessment of endolysosomal physiology. Curiously, they induce the conjugation of Atg8, a marker protein of autophagosomes, on the PE present in the limiting membrane of endosomes and its subsequent degradation in the vacuole lumen through a process that does not require several core ATG proteins. Our data thus suggest that Bph1 function is needed for efficient endosome biogenesis and regulation of the autophagy machinery.

RESULTS

Bph1 is an endosomal protein

Given that Bph1 is the only BEACH-domain-containing protein in yeast and is likely the ortholog of the LYST protein, we asked whether it functions in the biogenesis of the endolysosomal system. We initially assessed whether deletion of *BPH1* changed the morphology of the organelles in this system. We confirmed that deletion of *BPH1* did not change vacuole morphology by staining the vacuole membrane with the lipophilic dye FM4-64 (Fig. 1B) (Shiflett et al., 2004). We then determined the number of LEs in wild-type and *bph1Δ* mutant cells, by comparing the number of distinct puncta formed by endogenously GFP-tagged Vps8, a CORVET complex subunit, as a general LE marker protein. Recently, it has been described that yeast contains two separate subpopulations of LEs: multivesicular bodies (MVBs), which are characterized by the presence of endosomal complexes required for transport (ESCRT) complexes, and signaling endosomes (SEs), where a subpopulation of the TORC1 and Fab1 complexes and the

protein Ivy1 reside (Chen et al., 2021; Hatakeyama et al., 2019). We thus also examined the effect of *BPH1* deletion on these different types of endosomes, using the ESCRT-IV subunit Vps4 as a marker protein for MVBs and the protein Ivy1 as a marker protein for SEs. Although deletion of *BPH1* caused a minor reduction in the number of LEs marked by Vps8 (Fig. 1C,D), we conclude that the overall architecture of the endolysosomal system is not strongly affected (Fig. 1B–D; Fig. S1).

To uncover the precise localization of Bph1, we C-terminally tagged the protein with mNeonGreen (mNG). Determining the localization of Bph1 was challenging as the expression level of Bph1 is 5–10-fold less than that of any subunit of the tethering HOPS complex at the vacuole, which are already difficult to trace when endogenously GFP-tagged (Hönscher et al., 2014; Bröcker et al., 2012). The Bph1 protein appeared to have a cytosolic signal with accumulation in dots that colocalized with FM4-64-stained vacuolar membrane (Fig. 1E,F). Since LEs are often in close proximity to the vacuole (Day et al., 2018), we analyzed whether Bph1 puncta colocalized with Vps8 and found that approximately half of these puncta correspond to Vps8-positive LEs (Fig. 1E,F). In contrast, these puncta showed no overlap with mCherry-tagged marker proteins of the trans-Golgi network and early endosomes (Sec7), the endoplasmic reticulum (Sec63), or the nucleus–vacuole junction (Nvj1) (Fig. 1G).

Next, we analyzed to which subtype of LEs Bph1 localizes, MVBs or SEs (Chen et al., 2021; Hatakeyama et al., 2019). Bph1 dots also showed partial colocalization with the Vps4-positive MVBs and Ivy1-positive SEs, though we did not observe an exclusive enrichment to just one of these two LE subpopulations (Fig. 1E,F). We conclude that Bph1 localizes to both types of LEs as well as to dot-like structures in the proximity of the vacuole membrane, which are negative for the LE marker Vps8 and could represent a separate organelle or a subdomain of the vacuole.

Bph1 is an effector of the Rab5 isoform Ypt52

We next determined how Bph1 is recruited to LEs. The Rab5 isoforms Vps21 and Ypt52 localize to LEs, especially those adjacent to the vacuole (Day et al., 2018). As Rab GTPases are prime candidates to recruit peripheral membrane-associated proteins, we analyzed Bph1–mNG localization in strains in which different Rab5 isoforms had been deleted. Bph1 was distributed in puncta in the wild-type cells and in cells lacking Vps21 or Ypt10, the main Rab5 isoforms, but this dot-like localization appeared reduced in *ypt52Δ* cells (Fig. 2A,B; Fig. S2). This was surprising, as localization of known Vps21 effectors such as CORVET, BLOC1 or Mon1–Ccz1 is only abolished completely if Ypt52 is also deleted (Cabrera et al., 2013; Peter et al., 2013; Cabrera and Ungermann, 2013; Arlt et al., 2015; Paulsel et al., 2013), suggesting overlapping specificity between the two Rab5 isoforms. As Bph1–mNG appeared to be partially cytosolic, we selected the opposite approach by overexpressing Rab5 proteins, and observed that Bph1 accumulated in bigger and more intense puncta only when Ypt52 was overexpressed (Fig. 2C–E).

To determine whether Bph1 is indeed an effector of Ypt52, we purified Bph1 from yeast (Fig. S3) and added it to recombinant GST fusions of yeast Rab5 isoforms immobilized on glutathione beads in either their GDP- or GTP-loaded forms. We then eluted bound proteins and analyzed them by SDS–PAGE and western blotting against a TAP-tag fused to Bph1. Bph1 was only specifically retained on beads containing GTP–Ypt52 and was not retained on GDP–Ypt52 or any other Rab5 isoform (Fig. 2F). These data show that Bph1 is an effector of the Rab5 isoform Ypt52.

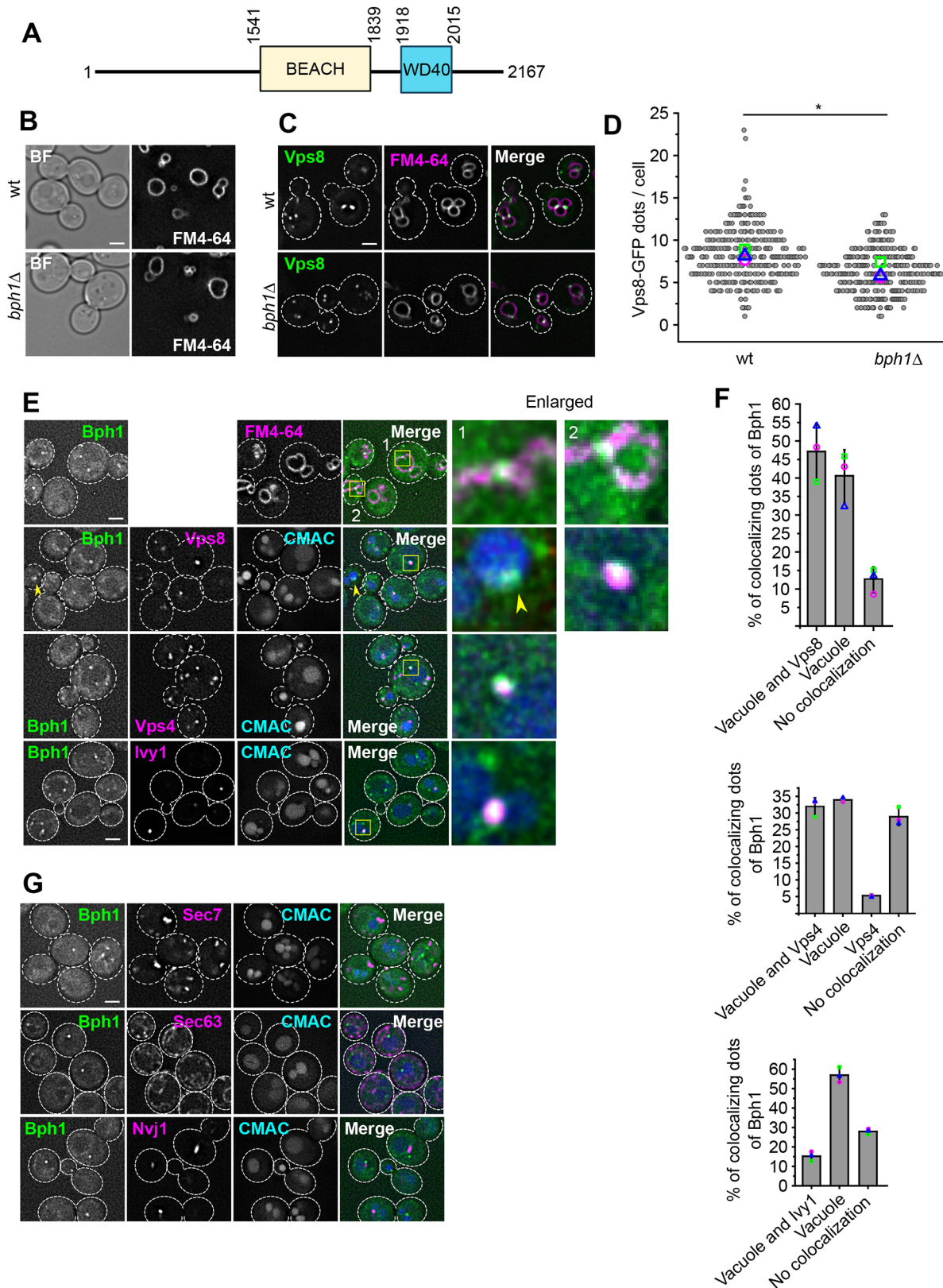


Fig. 1. See next page for legend.

As overexpression of Ypt52 caused Bph1 to accumulate in bigger structures, we asked whether these correspond to MVBs or SEs. We therefore co-expressed either Vps4-mCherry or Ivy1-mCherry in cells overexpressing Ypt52. In almost all

cases, Bph1 colocalized with Vps4, whereas Ivy1 dots were close by, but did not colocalize (Fig. 2G), indicating the Bph1 is found on Vps4-positive MVBs rather than SEs under these conditions.

Fig. 1. Bph1 is an endosomal protein. (A) Diagram depicting the domain organization of Bph1 with amino acid numbers indicated. (B) Vacuole morphology analysis. Wild-type (wt) and *bph1Δ* cells were grown to logarithmic phase, stained with the lipophilic dye FM4-64 and analyzed by fluorescence microscopy. BF, bright-field image. Scale bar: 2 μm. (C) Localization of Vps8. Vps8 was tagged C-terminally with mGFP in wild-type and *bph1Δ* cells. Cells were stained with FM4-64 and analyzed by fluorescence microscopy. Scale bar: 2 μm. (D) Quantification of the number of Vps8 dots per cell in the indicated strains. Each small circle represents one cell and the larger symbols represent the mean for each of three independent experiments. $n > 150$ cells $*P < 0.05$ (two-tailed unpaired Student's *t*-test). (E) Bph1 localization in cells. Bph1 was tagged C-terminally with mNG and analyzed in cells stained with FM4-64, or in cells co-expressing Vps8–mKate2, Vps4–mCherry or Icy1–mKate2 that were also stained with CMAC to visualize the vacuole. Boxes mark regions shown in enlarged images on the right. Arrowheads indicate Bph1 dots that colocalize exclusively with the vacuole. Scale bars: 2 μm. (F) Quantification of the percentage of Bph1 structures that colocalize with Vps8, Vps4 or Icy1. Data are presented as mean ± s.d. with the mean values of three independent experiments indicated. (G) Colocalization of Bph1 with other organellar markers. Cells expressing Bph1–mNG and mCherry-tagged Sec7 (Golgi), mKate2-tagged Sec63 (endoplasmic reticulum) or mKate2-tagged Nvj1 (nucleus–vacuole junction) were analyzed by fluorescence microscopy. Cells were stained with CMAC to visualize the vacuole. Scale bar: 2 μm. Dashed lines in C,E,G mark cell outlines.

To identify the molecular microenvironment of Bph1, we C-terminally tagged the protein with a TurboID tag to biotinylate proximal proteins (Branon et al., 2018). Due to the low abundance of Bph1, we again used the co-overexpression background of Bph1 and Ypt52 to isolate biotinylated proteins and determine their identity by protein mass spectrometry (Fig. 2H) (Schoppe et al., 2020). The identified proteins were analyzed in a volcano plot combining intensity ratios and significance in a two-group *t*-test (Fig. 2H). The complete list of proteins with their intensities, ratios and significance is presented in Table S2. In total, 141 proteins were identified as being significantly enriched in the sample containing TurboID-tagged Bph1. Analysis of this set of proteins showed a significant enrichment of cellular component Gene Ontology (GO) terms corresponding to endosomes and vacuole (marked in red and green, respectively, in Fig. 2H and Table S3). The complete list of significantly enriched cellular component GO terms is shown in Table S3. These data support our previous conclusions of LE localization of Bph1.

Bph1 is linked to Atg8 lipidation at LEs

To determine the function of Bph1 at LEs, we analyzed the functionality of several protein-sorting pathways in a strain lacking *BPH1*. In agreement with a previous analysis (Shiflett et al., 2004), *bph1Δ* cells did not show a defect in protein sorting from the Golgi to the vacuole via the AP-3 pathway or the carboxypeptidase Y (CPY) endosomal pathway (Fig. S4). We assessed the functionality of the AP-3 pathway by the intracellular distribution of a synthetic cargo that appears on the plasma membrane in addition to the vacuole membrane when the pathway is defective (Fig. S4A) (Schoppe et al., 2020). Trafficking through the endosomal CPY pathway was also unaffected, as assessed by the intracellular content of CPY, which is secreted when the pathway is defective (Fig. S4B).

We then asked whether Bph1 is involved in autophagy. A convenient marker protein to assess autophagy progression is a soluble form of the alkaline phosphatase Pho8 that lacks the first 60 residues containing its transmembrane domain (Guimaraes et al., 2015). Upon induction of autophagy by nitrogen starvation, the cytosolic Pho8Δ60 protein is non-specifically sequestered into forming autophagosomes and is delivered into the vacuole, in which Pho8Δ60 is processed into its active form by resident proteases.

High Pho8Δ60 activity thus reflects an autophagic activity, which is observed only upon starvation of cells (Fig. 3A). Using this assay, we analyzed *bph1Δ* cells and observed a 50% reduction in autophagic activity, which was rescued to almost wild-type levels by introducing a Bph1-encoding plasmid. Cells lacking Atg9, a key ATG protein, showed a complete block in autophagy, indicating that the assay is very sensitive to the loss of the core components (Fig. 3A). These reduced levels of Pho8 activity were not caused by decreased proteolytic activity of the vacuoles, which would thus fail to activate Pho8, as measurement of total alkaline phosphatase activity from vacuoles of wild-type and *bph1Δ* cells showed no significant difference (Fig. 3B).

To further analyze autophagy, we monitored the sorting of GFP-tagged Atg8 (Guimaraes et al., 2015; Klionsky et al., 2021). Upon induction of autophagy, Atg8 was found in the vacuole lumen in wild-type cells and *bph1Δ* cells, and the GFP–Atg8 fusion protein was proteolytically processed (Fig. 3C,D). This suggests that Bph1 affects autophagy only partially.

While monitoring the localization of GFP–Atg8 under normal growth conditions, we made a surprising observation. Whereas GFP–Atg8 localized to single perivacuolar dots in wild-type cells, which are very likely to be sites of autophagosome formation (Klionsky et al., 2021), *bph1Δ* cells had more Atg8-positive punctuate structures (Fig. 4A,B). Importantly, this knockout strain also accumulated Atg8 in the lumen of the vacuole, a phenotype that was rescued upon re-expressing Bph1 in the deletion mutant (Fig. 4A,B). We next asked how Atg8 reached the vacuole lumen. Under normal growth conditions, luminal sorting of proteins into the vacuole lumen can occur either via endosomal transport through MVBs, which requires ESCRT proteins (Henne et al., 2011); the cytosol-to-vacuole targeting (Cvt) pathway, a biosynthetic selective type of autophagy (Lynch-Day and Klionsky, 2010); or microautophagy (Oku et al., 2017; Schäfer et al., 2019; Dawaliby and Mayer, 2010). To determine whether ESCRT proteins are required, we knocked out *VPS4* in the *bph1Δ* strain. This completely prevented Atg8 sorting into the vacuole lumen (Fig. 4C), revealing that Atg8 is likely delivered into the vacuole by MVBs or microautophagy, which also depends on the ESCRT machinery (Schuck, 2020). The increased delivery of GFP–Atg8 to the vacuole lumen could also be observed as increased proteolysis of the fusion protein (Fig. 4D). Consistently with our microscopy results, this increased degradation was abolished by deletion of *VPS4* (Fig. 4D).

To ask whether the Cvt pathway was involved, we deleted either *ATG9* – the only transmembrane protein required for autophagy – or the Atg1 kinase, but neither deletion prevented Atg8 delivery into the vacuole lumen or the increased proteolysis of GFP–Atg8 in cells that lacked *BPH1* (Fig. 4E,F). A recently described pathway for the degradation of vacuolar membrane proteins in stationary phase involves unlipidated Atg8, ESCRT complexes and the Atg8 interactor Hfl1 (He et al., 2021). To test if this pathway was involved, we assessed the localization of mCherry–Atg8 in a double mutant lacking both *BPH1* and *HFL1*. Atg8 was still found in the vacuole lumen in this strain, indicating that it does not reach the vacuole through the Hfl1 pathway when Bph1 is missing (Fig. S5A).

If Atg8 is indeed directed into the vacuole through MVBs and not via microautophagy in the *bph1Δ* mutant, we would also expect Atg8 puncta to mark LEs under growing conditions. We therefore colocalized mCherry-tagged Atg8 with Vps8–mNG in wild-type and mutant cells. Whereas Vps8 and Atg8 marked separate dots in wild-type cells, they colocalized significantly in the *bph1Δ* mutant. This indicates that the *BPH1* deletion leads to a recruitment of Atg8 onto LEs (Fig. 5A,B). Consistent with Atg8 arriving to the vacuole

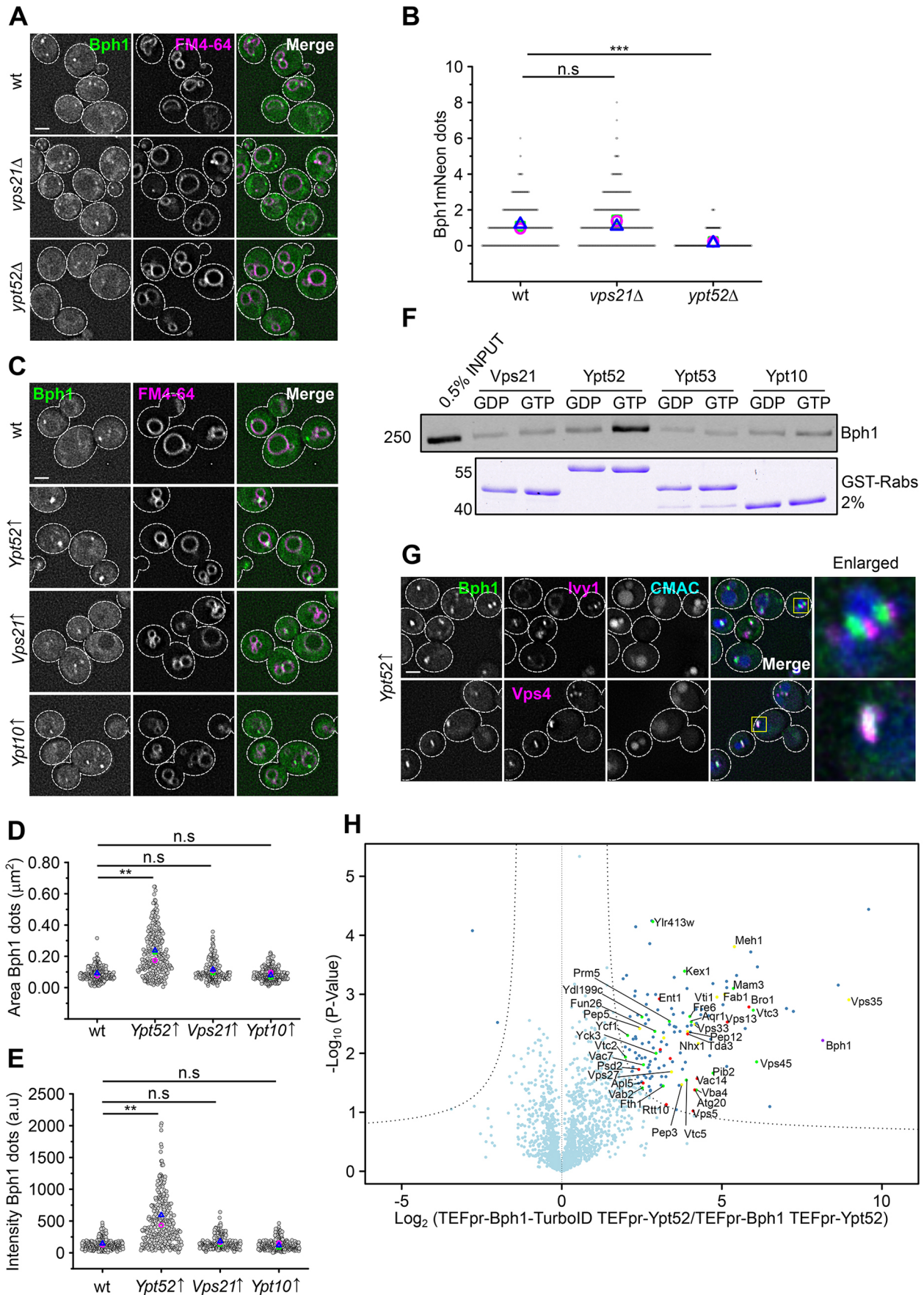


Fig. 2. See next page for legend.

Fig. 2. Bph1 is an effector of the endosomal Rab5 isoform Ypt52 and is proximal to multiple endolysosomal proteins. (A) Localization of Bph1 in Rab5 mutant strains. Bph1–mNG was expressed in wild-type (wt), *vps21Δ* and *ypt52Δ* cells that were stained with FM4-64 and analyzed by fluorescence microscopy. Scale bar: 2 μm. (B) Quantification of the number of Bph1–mNG dot-like structures per cell in wild-type cells and Rab5 mutants. Each small circle represents a cell, and the larger symbols represent the mean of each of three independent experiments. *** $P \leq 0.001$; n.s., not significant (two-tailed unpaired Student's *t*-test). (C) Effect of Rab5 overexpression on Bph1 localization. The indicated Rab5 isoforms were placed under the control of the strong constitutive *TEF1* promoter in cells expressing Bph1–mNG. Cells were stained with FM4-64 and then analyzed by fluorescence microscopy. Scale bar: 2 μm. (D,E) Quantification of the area of Bph1-positive dots (D) and the intensity of Bph1-positive dots (E) in the indicated strains (a.u., arbitrary units). Each small circle represents a cell, and the larger symbols represent the mean of each of three independent experiments. ** $P \leq 0.01$; n.s., not significant (two-tailed unpaired Student's *t*-test). (F) Purified Bph1 binds GTP–Ypt52. The indicated Rab GTPases were purified as GST fusion proteins from *E. coli*, immobilized on glutathione agarose and loaded with GDP or GTP. Rab-containing beads were then incubated with purified Bph1 and washed. Bound Bph1 was eluted by the addition of EDTA and 300 mM NaCl and was then analyzed by SDS–PAGE and western blotting (top). Equal amounts of beads containing Rab5 proteins were heated in SDS sample buffer, and samples were analyzed by SDS–PAGE and Coomassie staining (bottom). Data shown are representative of three independent experiments. Molecular mass is indicated in kDa. (G) Bph1 localizes to MVBs when Ypt52 is overexpressed. Bph1–mNG and either Ivy1–mCherry or Vps4–mCherry were expressed in cells overexpressing Ypt52 from the *TEF1* promoter. Cells were stained with CMAC to visualize the vacuole and were analyzed by fluorescence microscopy. Boxes indicate regions shown in enlarged images. Scale bar: 2 μm. Images are representative of one experiment. (H) Identification of proteins proximal to Bph1. Bph1 was tagged C-terminally with the TurboID tag in cells co-overexpressing Bph1 and Ypt52 from the *TEF1* promoter (TEFpr). Cells were incubated with biotin for 3 h, and biotinylated proteins were isolated on Streptavidin beads, eluted and analyzed by mass spectrometry. The volcano plot represents the results of the label-free pull downs. The logarithmic ratio of protein intensities in the samples in which Bph1 is tagged with TurboID/untagged samples were plotted against negative logarithmic *P*-values of the *t*-test performed for triplicate pull downs. Each dot in the volcano plot represents one identified protein, and the proteins above the hyperbolic dashed curves are considered significant. Significant proteins annotated with GO terms 'vacuole' (green), 'endosome' (red) or both (yellow) are marked and identified. Dashed lines in A,C,G mark cell outlines.

lumen through the MVB pathway and not through the induction of an additional specific pathway, the membrane structures observed inside the vacuole by ultrastructural analysis in a *bph1Δpep4Δ* strain did not differ from the ones observed in a *pep4Δ* strain, and completely disappeared in a *bph1Δvps4Δ* strain (Fig. S5B).

Since Atg8 association with membranes requires its conjugation to PE, we examined whether this modification was important to target Atg8 to LEs and the vacuole lumen in the absence of Bph1. Atg8 is posttranslationally processed by the Atg4 protease to expose a C-terminal glycine that is used for the conjugation to PE (Mizushima, 2020). GFP–Atg8 sorting into the vacuole lumen was abolished in the *bph1Δatg4Δ* double mutant (Fig. 5C), indicating that Atg8 targeting to LEs and the vacuole requires Atg8 lipidation. Consistently, deletion of *ATG4* also abolished the increased proteolysis of GFP–Atg8 in *bph1Δ* cells (Fig. 5D). To confirm this result, we also deleted Atg7, the E1 enzyme responsible for Atg8 activation during PE conjugation, and observed the same block (Fig. S6A).

To confirm these findings, we also monitored lipidation of endogenous Atg8 on gels. In wild-type cells, Atg8 appears in two forms in SDS–PAGE, the non-modified slower-moving Atg8 and the faster-moving Atg8-PE, which is a minor band under normal growth conditions and is more visible if the vacuolar protease Pep4 is deleted (Mizushima, 2020) (Fig. 5E). If cells are shifted to medium lacking nitrogen, Atg8-PE is the predominant Atg8 band,

reflecting the induction of autophagy. This is prevented in cells lacking the E1 enzyme Atg7. When we analyzed the *bph1Δ* mutant, we observed more Atg8-PE than in wild-type cells under normal growth conditions. This became far more obvious when we also deleted the major vacuolar protease *PEP4*, blocking the turnover of all the Atg8-PE produced (Fig. 5E), indicating that Atg8 is lipidated to a higher extent in *bph1Δ* cells under normal growth conditions. These data agree with the accumulation of Atg8 in the vacuole lumen (Fig. 4A).

For Atg8 to be lipidated on endosomal membranes and delivered to the vacuole via the MVB pathway when *BPH1* is lacking, the lipidation machinery must be recruited to endosomes under these conditions. We thus assessed the localization of Atg16 and Atg5 under growth conditions in cells lacking Bph1. The expression levels of both these proteins is very low under growth conditions, and they display a mainly cytosolic distribution with some dot-like accumulations (Fig. 5F,H). While these accumulations did not colocalize with the late endosomal marker Vps8 in wild-type cells, a significant portion of them did colocalize when *BPH1* was missing (Fig. 5F–I). The recruitment of the Atg8 lipidation machinery to endosomes in the absence of Bph1 explains the increased lipidation of Atg8, its localization to LEs and delivery to the vacuole lumen for degradation.

Bph1 function is required for efficient endocytosis and endosomal sorting

To clarify the effect of the lack of *BPH1* on sorting to the vacuole we used vacuolar proteomics, a method that we recently established as a tool to determine alterations in protein sorting due to selected deletions (Eising et al., 2019). We used stable isotope labeling by amino acids in cell culture (SILAC) to compare the vacuolar proteome of light-lysine-labeled wild-type cells with heavy-lysine-labeled *bph1Δ* cells (Fig. 6A; Table S4), as well as light-lysine-labeled *pep4Δ* and heavy-lysine-labeled *pep4Δbph1Δ* cells (Fig. 6B; Table S5), as this background allows us to detect proteins that are turned over too fast for detection in the wild-type background.

In agreement with our earlier analyses (Fig. 4A), we observed that vacuoles from the *bph1Δpep4Δ* mutant had an elevated amount of Atg8 compared to that in *pep4Δ* cells (Fig. 6B, right part of the plot). In addition, these vacuoles had more Atg27 as a sorting factor of Atg9 (Legakis et al., 2007), but were strongly deficient in all known Cvt pathway cargoes – such as Lap1 (also known as Ape2), Ape1 and Ape4 – and the receptor required for their sorting in this transport route, Atg19 (Fig. 6B, left part of the plot; Table S5) (Lynch-Day and Klionsky, 2010). This suggests that the degradation of Atg8 through the MVB pathway in *bph1Δ* cells may hinder the Cvt pathway, as the autophagy-related pathway active under growth conditions.

Additionally, we observed that *bph1Δ* mutants showed depletion of several plasma membrane proteins, including the transporters Zrt1, Mup1 and Gap1, suggesting a general endocytosis defect (Fig. 6A; Table S4). The methionine transporter Mup1 accumulates at the plasma membrane in the absence of methionine and is endocytosed and transported to the vacuole for degradation in the presence of methionine (Fig. 6C). This induction in Mup1 endocytosis allows the kinetics of this process to be followed using microscopy. In agreement with our vacuole proteomic analysis, we observed a delay in the transport of Mup1 toward the vacuole in *bph1Δ* cells (Fig. 6C,D). These results are also consistent with a previously reported mild hypersensitivity of *bph1Δ* cells to canavanine, a toxic analog of arginine, and to Calcofluor White, which we could also reproduce (Fig. 6E) (Shiflett et al., 2004).

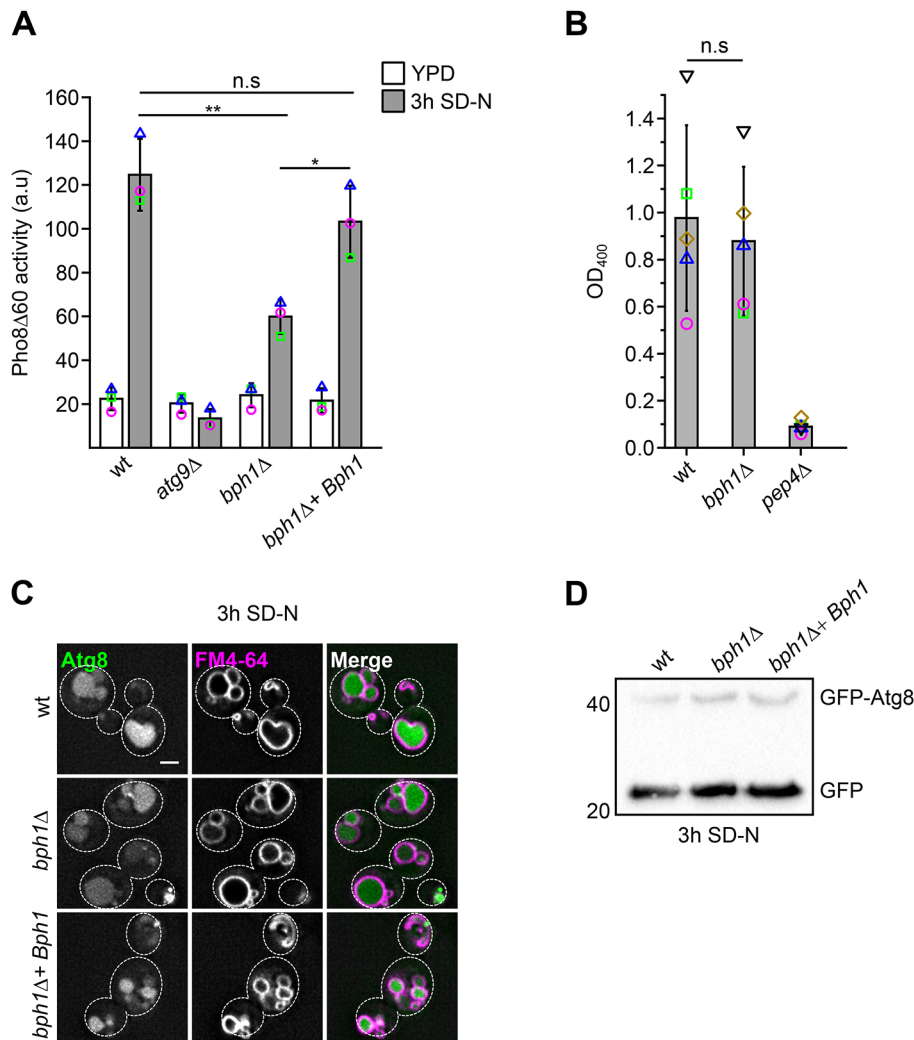


Fig. 3. Effect of *BPH1* deletion on autophagy.

(A) Analysis of autophagy via the Pho8Δ60 assay. The indicated cells (wt, wild type), expressing the Pho8Δ60 truncation, were grown in YPD and then shifted to minimal medium lacking nitrogen (SD-N) for 3 h. Pho8 activity was determined as described in the Materials and Methods (a.u., arbitrary units). Bph1 was expressed from a plasmid in *bph1Δ* cells (*bph1Δ*+Bph1). (B) Pho8 activity measurement of isolated vacuoles. Equivalent amounts of vacuoles from the indicated strains were lysed, and Pho8 activity was measured. The bar graphs in A and B correspond to the mean±s.d. (A, $n=3$; B, $n=5$), with mean values for the independent experiments indicated. * $P<0.05$; ** $P<0.01$; n.s., not significant (two-tailed unpaired Student's *t*-test). (C) Effect of nitrogen starvation on Atg8 localization. GFP-Atg8 was expressed in the indicated cells, which were grown in SD-N for 3 h to induce autophagy. Cells were stained with FM4-64 and analyzed by fluorescence microscopy. Dashed lines mark cell outlines. Images are representative of three independent experiments. Scale bar: 2 μm. (D) Analysis of GFP-Atg8 processing. Cells from the indicated strains transformed with a plasmid expressing GFP-Atg8 were grown to exponential phase and shifted to starvation medium (SD-N) for 3 h. Whole-cell lysates were analyzed by SDS-PAGE and western blotting with antibodies recognizing GFP. Blot shown is representative of three independent experiments. Molecular mass is indicated in kDa.

These results point to a trafficking defect of selected cargoes along the endocytic pathway.

Taken together, our data are consistent with a model in which the function of Bph1 at LEs as an effector of Ypt52 is necessary for normal endocytosis and sorting in the endosomal pathway. Lack of Bph1 results in the lipidation of Atg8 in LEs and its untimely degradation in the vacuole lumen under growth conditions (Fig. 6F).

DISCUSSION

In this study, we shed light on the function of the yeast LYST homolog, the BEACH-domain-containing protein Bph1. We demonstrate that Bph1 is an LE protein and an effector of the Rab5 isoform Ypt52, as shown by the effect of Ypt52 deletion and overexpression on the *in vivo* localization of Bph1, and by *in vitro* binding experiments. This notion is supported by proximity labeling of Bph1 and next-neighbor analyses by mass spectrometry (Fig. 2). Our data further reveal that Bph1 regulates specific LE functions, such as Atg8 conjugation to PE (Fig. 5). Cells lacking Bph1 have Atg8-PE on LEs, which is then delivered to the vacuole lumen via sorting into the intraluminal vesicles of MVBs. The notion of Bph1 being involved in specific LE functions is also supported by the observation that *bph1Δ* cells have a clear defect in endolysosomal trafficking of a subset of endocytosed proteins, as revealed by vacuolar proteomics and trafficking analysis of Mup1-GFP.

An understanding of Chediák–Higashi syndrome, a rare autosomal human disease, rests on our understanding of the affected LYST protein, whose function remains enigmatic (Sharma et al., 2019). LYST is a large protein with a long N-terminal α -helical segment, a BEACH domain and a β -propeller region (Cullinane et al., 2013). Unfortunately, the domain organization has not provided insights into the function of LYST. We have also attempted to analyze truncated variants of Bph1 to identify minimal domains required for Bph1 association with LEs or to rescue the Atg8 sorting phenotype, but we encountered major protein stability problems and thus obtained the same phenotypes as observed for the deletion mutant (data not shown). Several previous studies have suggested a role of LYST in fission or fusion at endosomes, because lack of the protein produces swollen lysosomes in human cells, flies and *Dictyostelium* (Holland et al., 2014; Rahman et al., 2012; Falkenstein and Lozanne, 2014; Sepulveda et al., 2015). Interestingly, these studies have not found significant defects in the transport of biosynthetic proteins to lysosomes, nor in endocytosis. Similarly, loss of Lvs1, the LYST homolog in *Schizosaccharomyces pombe*, results in large vacuoles (Rains et al., 2017).

Our analysis of yeast Bph1 sheds light on a possible function of LYST. Even though the vacuole morphology is not altered by *BPH1* deletion in yeast, vacuolar proteomics and growth analyses clearly show that they have a defect in the endocytosis of a subset of cargoes (Fig. 6). It is possible that this has been overlooked in previous analyses of LYST, in which model cargo proteins have been

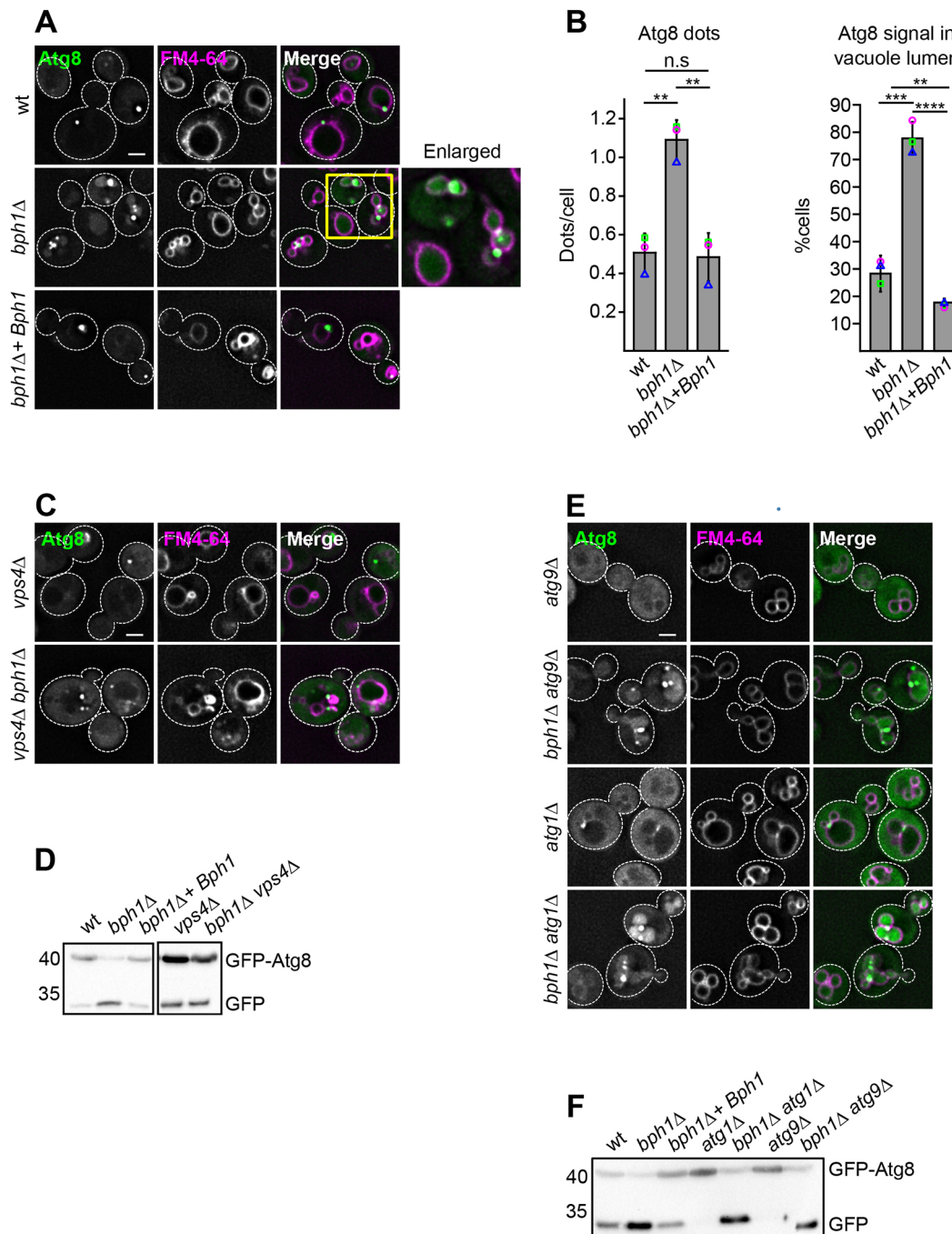


Fig. 4. Cells lacking Bph1 mislocalize Atg8 to the vacuole lumen. (A) Sorting of Atg8 to the vacuole lumen in *bph1Δ* cells under normal growth conditions. The indicated cells (wt, wild type) expressing GFP-Atg8 were stained with FM4-64 and analyzed by fluorescence microscopy. Box marks the region shown in the enlarged image. Scale bar: 2 μ m. (B) Quantification of Atg8-positive dots and Atg8 signal in the vacuole lumen in the indicated strains. Bar graphs show mean number of Atg8 dots per cell (left) or mean percentage of Atg8 signal in vacuole lumen (right), presented as mean \pm s.d. ($n=3$), with mean values each independent experiment indicated. ** $P \leq 0.01$; *** $P \leq 0.001$; **** $P \leq 0.0001$; ns, not significant (two-tailed unpaired Student's *t*-test). (C) Effect of the indicated deletions on GFP-Atg8 localization in *bph1Δ* cells. GFP-Atg8 was expressed in *vps4Δ*. Cells were stained with FM4-64 and analyzed by fluorescence microscopy. Scale bar: 2 μ m. (D) Analysis of GFP-Atg8 processing. The indicated strains carrying a *pRS415-pCuGFP-ATG8* plasmid were grown to logarithmic phase, and the whole-cell lysates were analyzed by SDS-PAGE and western blotting to detect GFP. (E) Localization of GFP-tagged Atg8 in strains harboring deletion of *atg9Δ* and *atg1Δ* without or with *BPH1* deletion. Cells were stained with FM4-64 and analyzed by fluorescence microscopy. Scale bar: 2 μ m. (F) Effect of indicated mutations on GFP-Atg8 processing. Cells were analyzed as in D. Data in C-F are representative of three independent experiments. Dashed lines in A, C, E mark cell outlines. In D and F, molecular mass is indicated in kDa.

analyzed to determine possible defects in endocytosis (Holland et al., 2014; Sepulveda et al., 2015; Rains et al., 2017; Falkenstein and Lozanne, 2014). In this regard, vacuolar proteomics provides a decisive advantage because it uncovers global changes in the

endogenous protein levels of purified vacuoles that occur due to the deletion of interest, and therefore it is far more sensitive than other approaches (Eising et al., 2019). Our finding can thus explain the previously reported sensitivity of *bph1Δ* cells to cell wall inhibitors

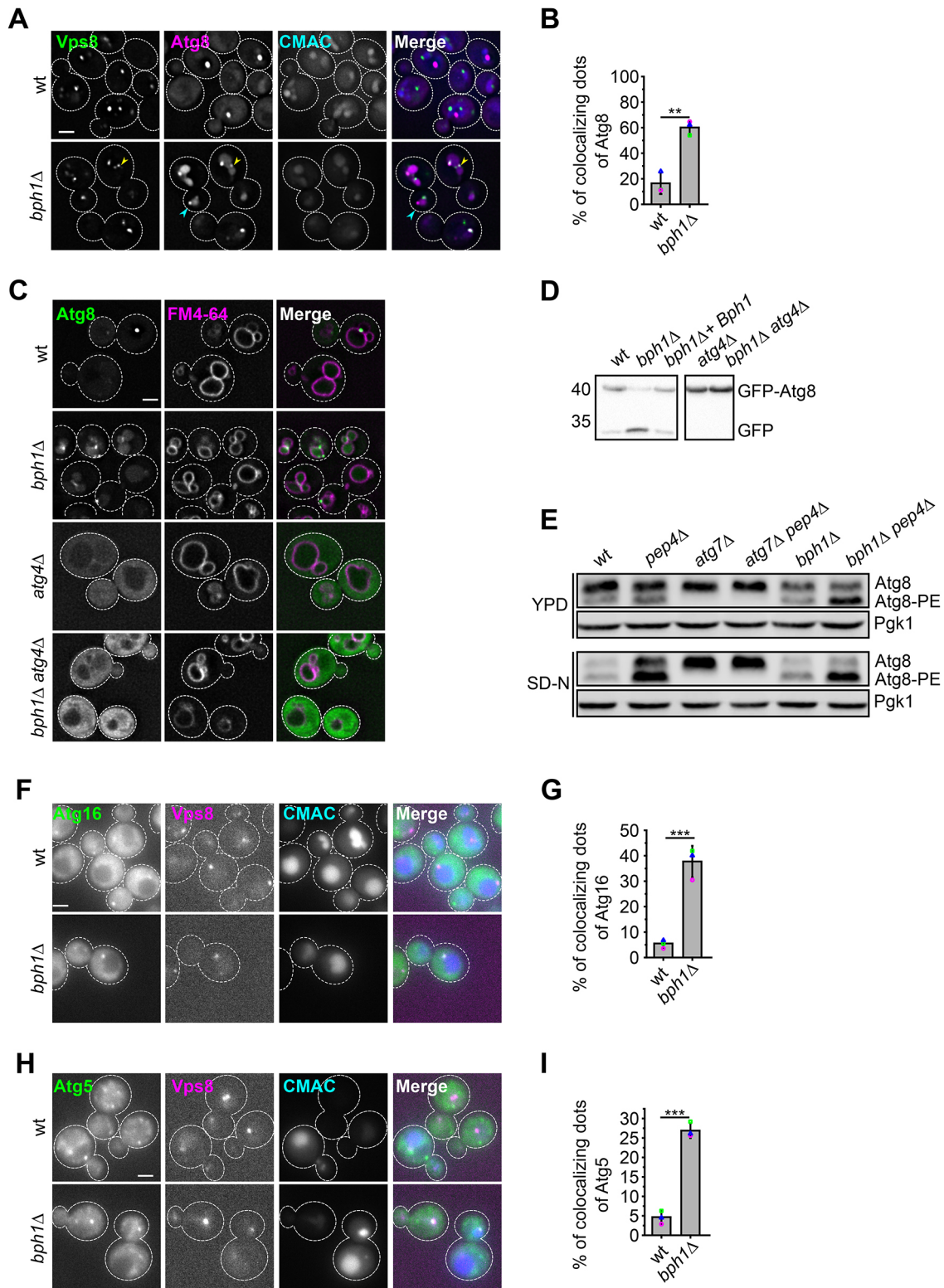


Fig. 5. See next page for legend.

such as Calcofluor White, which we could also reproduce, as the cell wall synthesizing enzymes are affected (Shiflett et al., 2004).

Moreover, we identify Bph1 as the first exclusive effector of the Rab5 isoform Ypt52 (Fig. 2). Previously, Vps21 has been considered as the main yeast Rab5 protein, whose function can be compensated by Ypt52 (Singer-Krüger et al., 1994; Horzodovsky

et al., 1994; Nickerson et al., 2012; Cabrera et al., 2013). Here, we find that Ypt52 has an exclusive function in binding Bph1. Ypt52 might be equivalent to the Rab4 homolog Ypt4 in *S. pombe*, as deletions in the LYST homolog Lvs1 and Ypt4 lead to similar phenotypes (Rains et al., 2017). Bph1 is, however, more critical than Ypt52, because *bph1Δ* cells, but not *ypt52Δ* cells, sort Atg8 into the

Fig. 5. Bph1 function is linked to Atg8 lipidation on endosomes.

(A) Localization of Vps8 in wild-type (wt) and *bph1Δ* cells relative to Atg8. Cells expressing mNG-tagged Vps8 and mCherry-tagged Atg8 were stained with CMAC to visualize the vacuole and analyzed by fluorescence microscopy. Yellow arrowhead indicates a Vps8 dot positive for Atg8. The blue arrowhead indicates a non-colocalizing dot. Scale bar: 2 μm. (B) Quantification of the percentage of Atg8 dots that colocalize with Vps8. Data are presented as mean ± s.d. from three independent experiments, with mean values for each independent experiment indicated. ** $P \leq 0.01$ (two-tailed unpaired Student's *t*-test). (C) Effect of Atg4 deletion on GFP–Atg8 localization. Analysis was performed as described in Fig. 4A. Scale bar: 2 μm. Images are representative of three independent experiments. (D) GFP–Atg8 amounts in the indicated mutants. The background strains carrying a *pRS415-pCuGFP-ATG8* plasmid were analyzed as described in Fig. 4D. Blots shown are representative of three independent experiments. (E) Atg8 lipidation analysis. The indicated strains were grown in YPD and then shifted to nitrogen deficient SD-N medium. Total cell extracts were analyzed by SDS–PAGE and western blotting using antibodies to Atg8 and to Pgk1 as a loading control. Bands for Atg8 and modified Atg8-PE are indicated. Blots shown are representative of three independent experiments. (F,H) Localization of Atg16 and Atg5 in wild-type and *bph1Δ* cells relative to Vps8. Cells expressing 2×mNG-tagged Atg16 (F) or Atg5 (H) and mKate2-tagged Vps8 were stained with CMAC to visualize the vacuole and analyzed by fluorescence microscopy. Scale bars: 2 μm. (G,I) Quantification of the percentage of Atg16 (G) or Atg5 (I) dots that colocalize with Vps8. Graphs show mean ± s.d. from three independent experiments, with mean values for each independent experiment indicated. *** $P \leq 0.001$ (two-tailed unpaired Student's *t*-test). Dashed lines in A,C,F,H mark cell outlines.

vacuole lumen (Fig. S6B). As Bph1 likely has additional binding sites to lipids and/or other proteins, a small amount of Bph1 on LEs might be sufficient for its function. It is also possible that minimal binding to Vps21 is sufficient to recruit Bph1 to endosomes in *ypt52Δ* cells. At this stage, we do not know how Bph1 functions on LEs. It is possible that it tethers membranes or coordinates the biogenesis of a subset of endosomes involved in recycling of plasma membrane proteins. As Bph1 localizes to bright Vps4-positive puncta, such a tethering function is possible. Having the purified protein in hand will allow us to test these hypotheses in future.

The most striking phenotype of the *bph1Δ* deletion is the sorting of Atg8 in the vacuole lumen under normal growth conditions. In particular, lipidated Atg8 is found on LEs and follows the MVB pathway to be delivered into the vacuole lumen. This unusual pathway has been described in the context of LC3-associated phagocytosis (LAP), a host defense pathway in metazoan cells that is induced by luminal pathogens and reactive oxygen species (Fischer et al., 2020; Herb et al., 2019). In LAP, the activity of a subset of autophagy proteins, including those composing the phosphatidylinositol 3-kinase complex and two autophagy-specific ubiquitin-like conjugation systems, leads to the conjugation of mammalian Atg8 homologs onto phagosomes, redirecting these phagosomes to directly fuse with lysosomes (Martinez, 2018; Heckmann and Green, 2019). Another similar process has been coined LC3-associated endocytosis (LANDO), where LC3 is found on Rab5-positive endosomes in the context of aggregate removal along the endocytic pathway in neurons (Heckmann et al., 2019). Furthermore, LC3 conjugation to PE at LEs and sorting into the internal vesicles of MVBs controls the secretion of RNA-binding proteins from cells via extracellular vesicles (Leidal et al., 2019). Our insights into the functions of LC3 and Atg8 are still expanding, as Atg8 not only binds multiple cargoes (Wilfling et al., 2020; Marshall et al., 2019; Liu et al., 2018; Hawkins and Klionsky, 2021; Mizushima, 2020; Zellner et al., 2021) but also affects the membrane shape once conjugated to PE (Maruyama et al., 2021).

Interestingly, damaging of endosomes is sufficient for LC3 recruitment (Lystad et al., 2019). As a result, defective endosomal

biogenesis may thus lead to Atg8 recruitment onto LEs in *bph1Δ* cells. Our data suggest that Atg8 conjugation to PE on membrane surfaces other than the autophagosome can also occur in yeast and could define a new function of Atg8 at endosomes. Under certain conditions such as the *BPH1* deletion, Atg8 lipidation at endosomes might be of importance for cellular physiology. It is thus possible that Atg8 lipidation functions as a compensatory mechanism within the endolysosomal system. Whether Atg8 then binds certain proteins or targets defective endosomes toward faster fusion with MVBs is not yet clear.

Loss of *BPH1* also affects autophagy. This is not due to a depletion of the Atg8 pool per se, as Atg8 overexpression did not rescue the observed defect (data not shown). However, it is possible that impaired endosomal biogenesis and the relocalization of Atg8 onto LEs have a negative synergetic effect that leads to a partial autophagy defect.

In summary, our data provide novel insights into Bph1 as a novel Rab5 effector at endosomes. They also reveal an unexpected link between Bph1 and Atg8 conjugation to PE in LEs, which suggests either a regulatory role of Bph1 in this process or a possible physiological response to endosomal damage. Future studies are necessary to uncover the functional importance of this link and its molecular details, which in addition to being relevant for our knowledge about the organization of the endolysosomal system, could also be crucial to understanding the pathophysiology of Chediak–Higashi syndrome and devising possible therapeutic approaches to cure this devastating disease.

MATERIALS AND METHODS**Yeast strains, plasmids and antibodies**

S. cerevisiae strains and plasmids used in this study are listed in Table S1. Genetic manipulations were made by homologous recombination of PCR-amplified cassettes (Janke et al., 2004) as described previously (Janke et al., 2004). The following antibodies were used: anti-TAP tag (1:1000; Invitrogen, CAB1001; RRID: AB_10709700), anti-Atg8 (1:3000; Abreu et al., 2017), anti-Pgk1 (1:7500; Sánchez-Wandelmer et al., 2017), anti-Tom40 (1:3000; gift of Walter Neupert, deceased), anti-GFP (1:1000; Roche, 11814460001), goat anti-mouse IgG conjugated to peroxidase (1:10,000; Thermo Fisher Scientific, 31430; RRID: AB_228307), DyLight 800 goat anti-rabbit-IgG (1:10,000; Thermo Fisher Scientific, 35571; RRID: AB_614947), Alexa Fluor 488- or Alexa Fluor 568-conjugated goat anti-mouse-IgG or anti-rabbit-IgG (1:7500).

Imaging of yeast cells using fluorescence microscopy

Cells were grown to exponential phase in yeast extract peptone dextrose (YPD) or synthetic complete medium supplemented with all amino acids (SDC) [0.675% (w/v) yeast nitrogen base without amino acids, 2.0% (w/v) glucose, 0.075% (w/v) CSM (MPBiomedicals)]. To induce starvation, yeast cells were transferred to synthetic minimal medium lacking nitrogen and containing 2% glucose (SD-N) for 3 h. Vacuoles were stained with 30 μM FM4-64 (Molecular Probes Inc., Eugene, OR) for 30 min. Cells were washed twice with fresh medium and incubated in medium without dye for 1 h (Vida and Emr, 1995). To stain the vacuole lumen, cells were incubated with 0.1 mM 7-amino-4-chloromethylcoumarin (CMAC; Invitrogen) for 15 min, followed by washing with SDC medium.

Cells were imaged live in SDC or SD-N media on a DeltaVision Elite imaging system based on an Olympus IX-71 inverted microscope equipped with a 100× N.A. 1.49 objective; an sCMOS camera (PCO, Kelheim, Germany); an InsightSSI illumination system; 4',6-diamidino-2-phenylindole, GFP, mCherry and Cy5 filters; and SoftWoRx software (Applied Precision, Issaquah, WA). Single plane or *z*-stack images with 0.2 μm spacing were deconvolved (SoftWoRx). All images were processed and quantified with ImageJ software (NIH, Bethesda, MD). One representative plane of the *z*-stack from a deconvolved image is shown in each figure.

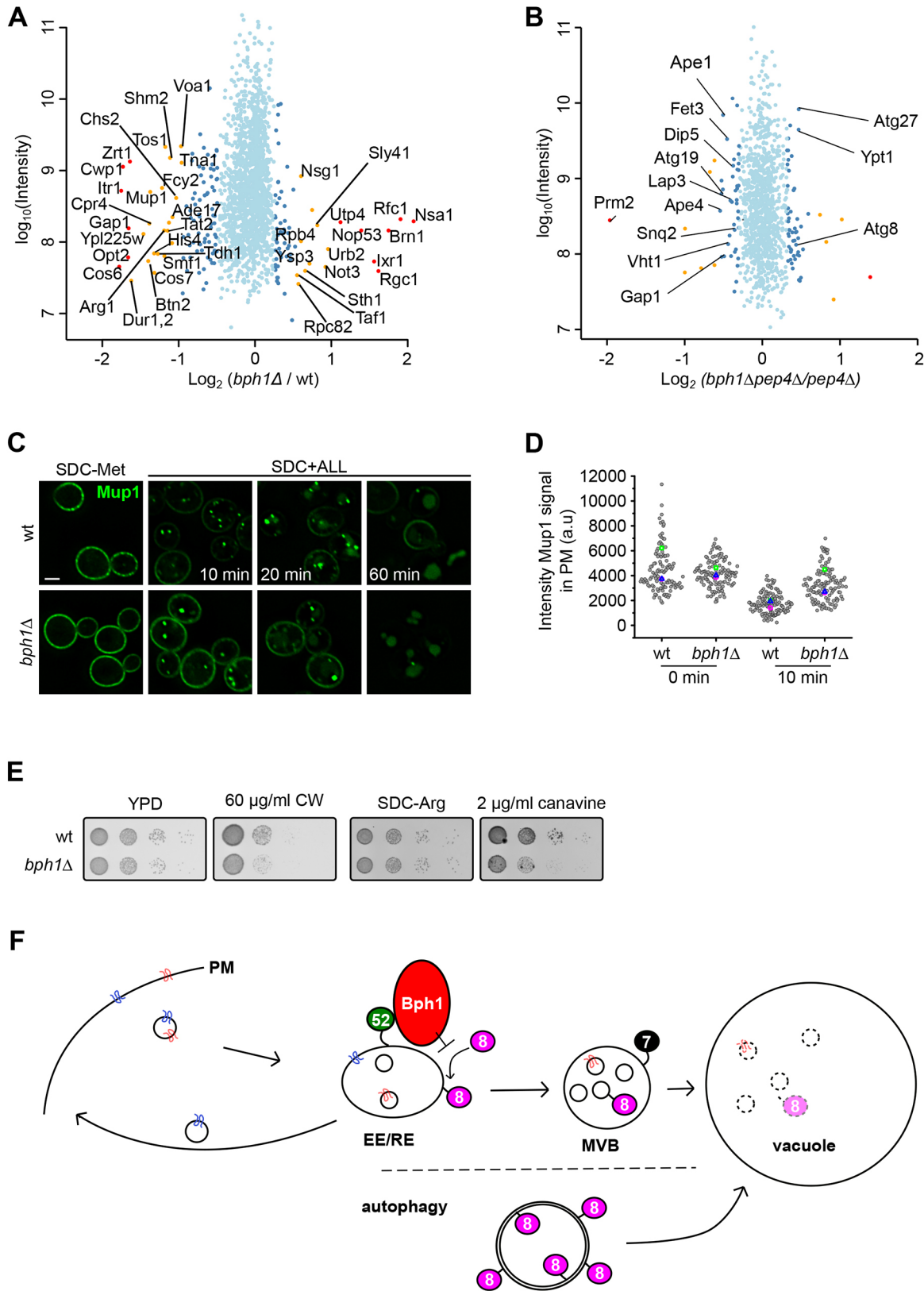


Fig. 6. See next page for legend.

Quantification

Details of quantification are also given in the figure legends. To analyze endosomal populations, endosomal dots per cell ($n \geq 100$) for three independent experiments were counted. This value for each cell is represented in the chart, as

well as the mean for each experiment, resulting in a superplot (Lord et al., 2020). The same procedure was used to quantify the number of Bph1 dots in wild-type and Rab5 deletion mutant cells. Statistical significance is based on an two-tailed unpaired Student's *t*-test between the means for each experiment.

Fig. 6. Bph1 is required for efficient endocytosis and involved in endosomal physiology.

(A,B) Vacuole proteomics reveals defects in the endocytic and Cvt pathways in cells lacking Bph1. Vacuoles were isolated from cells grown in media containing either heavy or light lysine, mixed in equimolar ratios and analyzed by mass spectrometry. (A) Light lysine, wild-type (wt) strain; heavy lysine, *bph1Δ* strain. (B) Light lysine, *pep4Δ* strain; heavy lysine, *pep4Δbph1Δ* strain. Identified proteins are shown according to their abundance (intensity, y-axis) and relative ratio (x-axis). Significant outliers ($P < 1 \times 10^{-14}$) are color coded in red; $P < 0.0001$, orange; $P < 0.05$, dark blue. Other identified proteins are shown in light blue. Protein names are shown for proteins with $P < 0.0001$. Data are representative of three independent experiments. (C) Endocytosis of Mup1. Mup1 was GFP-tagged in wild-type and *bph1Δ* cells. Cells were grown to log phase in synthetic medium lacking methionine (SDC-Met), imaged by fluorescence microscopy and then shifted to medium containing methionine (SDC+ALL). At the indicated time points, cells were analyzed as before by fluorescence microscopy. Scale bar: 2 μ m. (D) Quantification of Mup1-GFP localization to plasma membrane (PM). The intensity of the Mup1-GFP signal in the plasma membrane was plotted for each strain (a.u., arbitrary units). Small circles represent single cells, and the larger colored symbols represent the mean value for each of three independent experiments. (E) The indicated cells were grown to the same OD₆₀₀ and then spotted in serial dilutions (left to right) on YPD without or with Calcofluor White (CW), or on SDC-Arg without or with canavanine. Plates were grown at 30°C for 2–3 days before imaging. Images are representative of three independent experiments. (F) Model of Bph1 function at the endosome. Ypt52 (green), Ypt7 (black) and Atg8 (pink) are indicated by their numbers on endosomes. Atg8 sorting in autophagy is indicated at the bottom. EE, early endosome; RE, recycling endosome. For details, see the main text.

For colocalization experiments, the number of Bph1 dots that were positive for the indicated marker were counted. The percentage of these structures in each category, based on total number of dots, was calculated and represented in columns. Bars show the mean percentage of colocalizing dots \pm s.d. ($n \geq 100$), with means for each independent experiment also indicated.

To calculate area and intensity of Bph1-mNG-positive dots, ImageJ was used. A binary mask was created in a 16-bit image by applying a threshold filter (Default filter). The original picture was multiplied per the resulting binary mask, and the structures were measured for area and intensity. Values corresponding to area and intensity for three independent experiments were plotted as described above, with mean values for each experiment also represented in the same chart.

To measure the intensity of Mup1-GFP signal in plasma membrane, a line profile was drawn across the mother cell using ImageJ, and the two highest values were chosen to calculate the average of intensity in the plasma membrane. Results corresponding to three independent experiments are represented in a graph, as described above.

Ultrastructural analysis using electron microscopy

SEY6210 *pep4Δ*, *pep4Δvps4Δ* or *pep4Δbph1Δ* cells were cultured in YPD, and 15 OD₆₀₀ unit-equivalents of cells in log phase were harvested by centrifugation at 3000 *g* for 5 min at room temperature (RT). Cells were then washed once with 10 ml of distilled water. Cell pellets were subsequently resuspended in 1 ml of freshly prepared ice-cold 1.5% KMnO₄ (AppliChem; A3876, 0250) and transferred into microcentrifuge tubes. The microcentrifuge tubes were entirely filled with ice-cold 1.5% KMnO₄ to exclude air and were incubated on a slowly rotating wheel for 30 min at 4°C. Cells were then centrifuged at 1700 *g* for 3 min at 4°C, and the supernatant was discarded. Pellets were again resuspended in 1.5 ml of ice-cold 1.5% KMnO₄, and microcentrifuge tubes containing the samples were incubated on a rotating wheel overnight at 4°C. After five washes with 1 ml of distilled water, cells were collected by centrifugation at 1700 *g* for 3 min. Dehydration was performed by incubating the cells in 1 ml of 10%, 30%, 50%, 70%, 90% and 95% acetone (acetone for analysis ENSURE[®]; ACS, ISO, Reag. Ph Eur, 1.00014.1000) with at least 20 min incubations at RT. Between each incubation step, cells were collected by centrifugation at 2650 *g* for 4 min. Cells were then incubated three times in 1 ml of water-free acetone (dried acetone; MERCK, 1.00299.0500) for at least 20 min each time, on a slowly

rotating wheel at RT. This was followed by incubation in 33% freshly made Spurr's resin in acetone on a slowly rotating wheel for at least 1 h at RT. The Spurr's resin mixture was prepared mixing 26 g 2-nonen-1-yl succinic anhydride (Sigma, 74378), 10 g vinylcyclohexene dioxide (Fluka, 94956), 4 g diglycidyl ether of poly(propylene glycol) 736 (Fluka, 31191) and 0.2 g dimethylaminoethanol (Riedel-de-Haën[™], 15448). Cells were collected by centrifugation at 2650 *g* for 5 min and the supernatants discarded. Following this, cells were incubated in 100% Spurr's resin on a rotating wheel overnight at RT and collected by centrifugation at 2650 *g* for 5 min, after which the supernatant was discarded. Incubation in 100% Spurr's resin was repeated for 6 h at RT, and the samples were then transferred to conic embedding capsules (BEEM embedding capsules size 00; EMS, 70010-B). The capsules were centrifuged at 2650 *g* for 5 min and the supernatant discarded. The tubes were then topped with fresh 100% Spurr's resin and heated at 70°C for 4 days to polymerize the resin.

Ultra-thin 55 nm sections were cut using an UC7 Leica ultramicrotome (Leica Microsystems) and collected on carbon-coated formvar 50 meshes copper grids (EMS). Cell sections were stained with a filtered lead-citrate solution (80 mM lead nitrate, 120 mM sodium citrate, pH 12) for 2 min at RT. Sections were viewed using a Talos F200i transmission electron microscope (Thermo Fisher Scientific).

Expression and purification of GST-tagged Rab GTPases

Plasmids encoding GST-TEV-Vps21, GST-TEV-Ypt52, GST-TEV-Ypt53 and GST-TEV-Ypt10 were transformed into *E. coli* BL21 (DE3) Rosetta cells. Cells were grown to an OD₆₀₀ of 0.6, and expression was induced with 0.25 mM of IPTG overnight at 16°C. After harvesting, pellets were resuspended in purification buffer (50 mM HEPES-NaOH, pH 7.5, 150 mM NaCl, 1 mM MgCl₂, 1 mM DTT) with 1 mM phenylmethylsulfonyl fluoride (PMSF) and 1 \times protease inhibitor cocktail (0.1 mg/ml leupeptin, 1 mM o-phenanthroline, 0.5 mg/ml pepstatin A, 0.1 mM Pefabloc). Cells were lysed in a Microfluidizer, Model M-110L (Microfluidics, Newton, MA), and the resulting lysate was clarified by centrifugation at 40,000 *g* for 25 min at 4°C. Cleared lysates were incubated with pre-equilibrated Glutathione Sepharose (GSH) beads for 2 h at 4°C. Beads were washed three times with purification buffer, and proteins were eluted using purification buffer with 20 mM glutathione. Proteins were dialyzed overnight in dialysis buffer (50 mM HEPES-NaOH, pH 7.5, 150 mM NaCl, 1 mM MgCl₂). Dialysis buffer was changed twice.

Tandem affinity purification

Purification was carried out as previously described (Ostrowicz et al., 2010; Bröcker et al., 2012) with modifications. Cells expressing Bph1-TAP under the control of the *GAL1* promoter were grown overnight in yeast peptone (YP) medium with 2% (v/v) of galactose (YPG), diluted and grown for 24 h at 30°C to an OD₆₀₀ of 8. Cells were harvested by centrifugation (4800 *g*, 6 min, 4°C) and washed with 100 ml of cold water. Pellets were resuspended in TAP buffer (50 mM HEPES-NaOH, pH 8, 600 mM NaCl, 1.5 mM MgCl₂, 1 mM DTT) with 0.5 mM PMSF and 1 \times FY protease inhibitor mix (Serva, Germany). Liquid nitrogen was used to freeze the resuspension as small drops. Droplets were lysed in a Freezer Mill 6875D (SPEXsamplePrep) in 10 cycles each 2 min at 12 counts per second. The powder was thawed and resuspended in TAP buffer then incubated for 1 h at 4°C. The lysate was then centrifuged at 30,000 *g* for 10 min at 4°C. Cleared lysate was incubated with pre-equilibrated IgG Sepharose beads (GE, Germany) for 2 h at 4°C. Beads were washed in a column with 20 ml TAP buffer. Bound proteins were eluted by TEV (from our own purifications) cleavage overnight at 4°C.

GST pulldown and Rab interactions

Pulldowns of GST-tagged Rab5 proteins and purified Bph1 was performed as previously described (Langemeyer et al., 2020) with modifications. GST-tagged Rab5 GTPases (75 μ g per sample) were incubated with 250 μ l of buffer containing 20 mM HEPES-NaOH, pH 7.4, 20 mM EDTA, and 1 mM GDP or GTP (Sigma Aldrich, Germany). Samples were incubated for 15 min at 30°C and then adjusted to 25 mM MgCl₂ and 7 mg/ml bovine serum albumin. Next, 25 μ l of GSH-Sepharose 4B (GE Healthcare) was washed twice with buffer containing 20 mM HEPES-NaOH, pH 7.4, 1 mM

MgCl₂, 5% (v/v) glycerol and 0.1% (v/v) Triton X-100. Rab5 proteins were added and incubated for 1 h at 4°C. After incubation, samples were centrifuged for 1 min at 2000 *g*, GSH beads were retained, and the supernatant was discarded. Pulldown was performed in the presence of pulldown buffer [20 mM HEPES-NaOH, pH 8, 1 mM MgCl₂, 5% (v/v) glycerol 0.1% (v/v) Triton X-100, 300 mM NaCl], 1 mM of the corresponding nucleotide, 7 mg/ml BSA and 25 µg Bph1. The samples were incubated for 2 h at 4°C on a turning wheel. Beads were washed three times with 1 ml pulldown buffer. To elute bound proteins, 300 µl elution buffer [20 mM HEPES-NaOH, pH 8, 300 mM NaCl, 20 mM EDTA, 5% (v/v) glycerol and 0.1% (v/v) Triton X-100] was added for 20 min at RT on a turning wheel. Samples were briefly centrifuged to pellet the beads (1 min at 2000 *g*), the supernatant was precipitated by addition of trichloroacetic acid (TCA), and proteins were analyzed by SDS-PAGE and western blotting. For this, 0.5% of the input fraction and 100% of the elution fraction were loaded onto a gel. To compare amounts of bound Rab GTPases, 2× Laemmli buffer was added to GSH-Sepharose, and samples were heated for 10 min at 95°C, before 2% of the samples were analyzed by SDS-PAGE and Coomassie staining.

Analysis of Atg8 lipidation and GFP-Atg8 processing using western blotting

Cell extracts were prepared as described previously (Guimaraes et al., 2015). A total of 2.5 OD₆₀₀-equivalent units were harvested after 0 and 1 h starvation by centrifugation at 13,000 *g* for 1 min. Pellets were washed once with water and resuspended in 400 µl TCA (10% final concentration). After 30 min incubation on ice, pellets were spun down at 13,000 *g* for 5 min, and supernatants were discarded. Precipitates were resuspended in 100% ice-cold acetone and incubated for 20 min at -20°C. Samples were centrifuged, and pellets were dried at RT. Pellets were resuspended in SDS sample buffer [0.12 M Tris-HCl pH 6.8, 4% (w/v) SDS, 10% (v/v) glycerol, 0.01% (w/v) Bromophenol Blue, 2.5% (v/v) β-mercaptoethanol] and sonicated. Samples were then heated at 95°C for 5 min and loaded onto an SDS-PAGE gel containing 6 M urea. To analyze the levels of GFP-Atg8, samples were loaded onto a Bis/Tris SDS-PAGE gel. For western blotting, proteins were transferred to a nitrocellulose membrane (GE Healthcare, cat # 10600002). The membrane was blocked with 5% (w/v) milk powder (Roth, 68514-61-4) dissolved in 1× PBS buffer (8 mM Na₂HPO₄, 1.5 mM KH₂PO₄, 3 mM KCl, 140 mM NaCl) for 1 h. Then, the membrane was incubated with the primary antibody for 1 h at room temperature or overnight at 4°C followed by two washes with 1× TBS-Tween buffer [10 mM Tris-HCl pH 7.4, 155 mM NaCl, 0.5% (v/v) Tween 20] and three washes with 1× PBS, 5 min each. After washing, the membrane was incubated with the secondary antibody and washed as before.

SILAC labeling, vacuole isolation and proteomics

Control and mutant lysine-auxotroph strains were grown to logarithmic phase in 500 ml SDC-lysine medium (2% glucose, 6.7 g/l yeast nitrogen base without amino acids, 1.92g/l yeast synthetic dropout without lysine; Sigma-Aldrich) containing 30 mg/ml (final concentration) of either L-lysine (K0) or ¹³C₆, ¹⁵N₂ L-lysine (K8) (Cambridge Isotope Laboratories, USA). The same OD₆₀₀ units from each culture were mixed, and vacuoles were isolated as described previously (Haas, 1995). Protein concentration was determined by Roti-Quant (Roth). A commercial proteomics kit (iST Kit, proteomics) was used to prepare protein samples for mass spectrometry. A total of 200 µg of vacuoles was precipitated with TCA, and pellets were dissolved in lysis buffer from the kit. Proteins were digested with LysC according to the kit protocol. LC-load buffer from the kit was used to resuspend digested peptides.

Label-free pulldown of biotinylated protein

Cells co-overexpressing Bph1 and Ypt52 under control of the *TEF1* promoter and cells co-overexpressing Bph1-TurboID and Ypt52 were grown overnight to an OD₆₀₀ of 0.2 in 500 ml of Yeast Nitrogen Base (YNB) without amino acids and biotin (Formedium), supplemented with yeast synthetic drop-out media supplements without lysine (Sigma),

30 µg/ml L-lysine, 2% glucose and 0.125 ng/ml (final concentration) biotin (Novabiochem). Biotin to a 100 mM final concentration was added, and cells were grown to logarithmic phase (OD₆₀₀ 0.7–1). A total of 350 OD₆₀₀-equivalent units were harvested by centrifugation at 3000 *g* for 5 min and split into two tubes. Pellets were resuspended in 650 µl of lysis buffer A (20 mM Tris-HCl, pH 8, 1% SDS, 1 mM DTT) with 500 µl of glass beads (diameter = 0.4–0.6 mm) and lysed in a FastPrep Homogenizer (MP Biomedicals). Lysates were heated at 60°C for 10 min and separated from the glass beads by filtration. Then, 650 µl of lysis buffer B (8 M urea, 20 mM Tris-HCl, pH 8, 0.5% SDS, 1 mM DTT) was added to the lysates, and the mixture was centrifuged at 20,000 *g* for 20 min. The protein concentration was determined by Roti-Quant (Roth), and an equal amount of protein was used for each pulldown. 150 µl of streptavidin agarose resin beads (Thermo Scientific) were equilibrated with buffer C (mixture of buffer A and B, 1:1) and then incubated with lysates for 1 h at RT. Beads were washed four times with buffer C and four times with buffer C without DTT and SDS. Pulldown samples were processed following a standard on-bead digest protocol from a commercial proteomics kit (iST Kit, proteomics).

Mass spectrometry and analysis

Peptides were separated by reverse-phase chromatography on a Thermo Ultimate 3000 RSLCnano with a 50-cm PepMap C18 easy spray column (Thermo) with an inner diameter of 75 µm at a constant temperature of 40°C. Peptides were eluted from the column with a linear gradient of acetonitrile from 12 to 35% in 0.1% formic acid for 70 min, from 35 to 60% for 20 min, and from 60 to 90% for 15 min at a constant flow rate of 200 nl/min for the vacuole proteomics experiments. For the TurboID experiments, peptides were eluted from the column with a linear gradient of acetonitrile from 1 to 35% in 0.1% formic acid for 75 min, from 35 to 60% for 15 min, and from 60 to 90% for 14 min at a constant flow rate of 200 nl/min. Peptides eluting from the column were directly electrosprayed into a Q Exactive Plus mass spectrometer (Thermo). Mass spectra were acquired in a data-dependent mode to automatically switch between full MS scan and up to ten data-dependent MS/MS scans. The maximum injection time for full scans was 50 ms, with a target value of 3,000,000 at a resolution of 70,000 at *m/z*=200. The ten most intense multiply charged ions (*z*=2) from the survey scan were selected with an isolation width of 1.6 Th and fragment with higher energy collision dissociation (Olsen et al., 2007) with normalized collision energies of 27. Target values for MS/MS were set at 100,000 with a maximum injection time of 120 ms at a resolution of 17,500 at *m/z*=200. To avoid repetitive sequencing, the dynamic exclusion of sequenced peptides was set at 20 s.

The resulting MS and MS/MS spectra were analyzed using MaxQuant (version 1.6.17.0, www.maxquant.org; Cox and Mann, 2008; Cox et al., 2011) as described previously (Fröhlich et al., 2013). The search was performed using the *Saccharomyces cerevisiae* proteome (UP000002311) from UniprotKB release 2021-01. The search included carbamidomethylation of cysteine as a fixed modification. Lysine biotinylation (C₁₀H₁₄N₂O₂S; mass change 226.077598394) was added as a variable modification for the TurboID experiments. The maximum allowed mass deviation was 6 ppm for MS peaks and 20 ppm for MS/MS peaks. The false discovery rate was determined by searching a reverse database. The maximum false discovery rate was 0.01 on both the peptide and the protein level. The minimum required peptide length was six residues. For the vacuole proteomics experiments, the SILAC ratios were calculated with MaxQuant. TurboID experiments were performed in triplicates and analyzed using the label-free quantification option of MaxQuant (Cox et al., 2014) using the ‘match between runs option’. Calculations and plots were performed with the R software package (www.r-project.org; RRID:SCR_001905) following available label-free quantification scripts (Hubner et al., 2010).

For the TurboID experiment, a cut-off for significantly enriched proteins was set at a *P*-value of 0.05 and the SO parameter (curve bend) as defined in Hubner et al. (2010) was set to 1. The proteins identified as significant with these parameters were analyzed for Cellular Component GO term enrichment using YeastMine (Balakrishnan et al., 2012) with a cut-off *P*-value of 0.05 using a Holm–Bonferroni test.

Spotting assays

For growth tests, cells were grown in YPD or SDC without arginine (SDC-Arg) to logarithmic phase, diluted to an OD₆₀₀ of 0.25, and spotted in serial (1:10) dilutions onto plates made with either YPD, YPD containing 60 µg/ml Calcofluor White or SDC-Arg supplemented with 2 µg/ml of canavanine. Plates were incubated at 30°C for 1–4 days and then imaged.

Statistical analysis

Statistical analyses were performed with Origin Pro 9 software. Where indicated, the relevant statistical test that was implemented is mentioned in the figure legends. The level of significance was as follows: * $P \leq 0.05$; ** $P \leq 0.01$; *** $P \leq 0.001$; **** $P \leq 0.0001$.

Acknowledgements

We would like to thank Angela Perz and Kathrin Auffarth for technical assistance as well as members of the involved groups for helpful discussions.

Competing interests

The authors declare no competing or financial interests.

Author contributions

Conceptualization: P.V.D., A.G.M., C.U.; Methodology: P.V.D., R.H., M.M., S.W., F.F.; Investigation: P.V.D., R.H., M.M., S.W., F.F.; Data curation: P.V.D., R.H., S.W., F.R., F.F., A.G.M., C.U.; Writing – original draft: A.G.M., C.U.; Writing – review & editing: P.V.D., R.H., F.R., F.F., A.G.M., M.M., C.U.; Visualization: P.V.D., A.G.M.; Supervision: F.F., F.R., A.G.M., C.U.; Project administration: C.U., A.G.M.; Funding acquisition: F.R., F.F., A.G.M., C.U.

Funding

This work was funded by a grant of the Deutsche Forschungsgemeinschaft (UN111/13-1 to C.U.). P.V.D. received support from Deutsche Forschungsgemeinschaft SFB 944. F.F. and A.G.M. were supported by the Deutsche Forschungsgemeinschaft SFB 944 (project P20 to F.F., P25 to A.G.M.). F.R. received funding from ZonMw TOP (91217002), Nederlandse Organisatie voor Wetenschappelijk Onderzoek Open Competition ENW-KLEIN (OCENW.KLEIN.118) and H2020 Marie Skłodowska-Curie Actions ETN (765912) grants.

Peer review history

The peer review history is available online at <https://journals.biologists.com/jcs/article-lookup/doi/10.1242/jcs.259421>.

References

- Abreu, S., Kriegenburg, F., Gómez-Sánchez, R., Mari, M., Sanchez-Wandelmer, J., Rasmussen, M. S., Guimarães, R. S., Zens, B., Schuschnig, M., Hardenberg, R. et al. (2017). Conserved Atg8 recognition sites mediate Atg4 association with autophagosomal membranes and Atg8 deconjugation. *EMBO Rep.* **18**, 765–780. doi:10.15252/embr.201643146
- Arlt, H., Reggiori, F. and Ungermann, C. (2015). Retromer and the dynam Vps1 cooperate in the retrieval of transmembrane proteins from vacuoles. *J. Cell Sci.* **128**, 645–655.
- Balakrishnan, R., Park, J., Karra, K., Hitz, B. C., Binkley, G., Hong, E. L., Sullivan, J., Micklem, G. and Cherry, J. M. (2012). YeastMine—an integrated data warehouse for *Saccharomyces cerevisiae* data as a multipurpose tool-kit. *Database* **2012**, bar062. doi:10.1093/database/bar062
- Barr, F. A. (2013). Rab GTPases and membrane identity: Causal or inconsequential? *J. Cell Biol.* **202**, 191–199. doi:10.1083/jcb.201306010
- Bowman, S. L., Bi-Karchin, J., Le, L. and Marks, M. S. (2019). The road to lysosome-related organelles: insights from Hermansky-Pudlak syndrome and other rare diseases. *Traffic* **20**, 404–435. doi:10.1111/tra.12646
- Branon, T. C., Bosch, J. A., Sanchez, A. D., Udeshi, N. D., Svinikina, T., Carr, S. A., Feldman, J. L., Perrimon, N. and Ting, A. Y. (2018). Efficient proximity labeling in living cells and organisms with TurboID. *Nat. Biotechnol.* **36**, 880–887. doi:10.1038/nbt.4201
- Bröcker, C., Kuhlee, A., Gatsogiannis, C., kleine Balderhaar, H. J., Hönscher, C., Engelbrecht-Vandré, S., Ungermann, C. and Raunser, S. (2012). Molecular architecture of the multisubunit homotypic fusion and vacuole protein sorting (HOPS) tethering complex. *Proc. Natl. Acad. Sci. USA* **109**, 1991–1996. doi:10.1073/pnas.1117797109
- Cabrera, M. and Ungermann, C. (2013). Guanine nucleotide exchange factors (GEFs) have a critical but not exclusive role in organelle localization of Rab GTPases*. *J. Biol. Chem.* **288**, 28704–28712. doi:10.1074/jbc.M113.488213
- Cabrera, M., Arlt, H., Epp, N., Lachmann, J., Griffith, J., Perz, A., Reggiori, F. and Ungermann, C. (2013). Functional separation of endosomal fusion factors and the class C core vacuole/endosome tethering (CORVET) complex in endosome biogenesis*. *J. Biol. Chem.* **288**, 5166–5175. doi:10.1074/jbc.M112.431536
- Charette, S. J. and Cosson, P. (2007). A LYST/beige homolog is involved in biogenesis of Dictyostelium secretory lysosomes. *J. Cell Sci.* **120**, 2338–2343. doi:10.1242/jcs.009001
- Chen, Z., Malia, P. C., Hatakeyama, R., Nicastro, R., Hu, Z., Péli-Gulli, M.-P., Gao, J., Nishimura, T., Eskes, E., Stefan, C. J. et al. (2021). TORC1 Determines Fab1 Lipid Kinase Function at Signaling Endosomes and Vacuoles. *Curr. Biol.* **31**, 297–309.e8. doi:10.1016/j.cub.2020.10.026
- Cox, J. and Mann, M. (2008). MaxQuant enables high peptide identification rates, individualized p.p.b.-range mass accuracies and proteome-wide protein quantification. *Nat. Biotechnol.* **26**, 1367–1372. doi:10.1038/nbt.1511
- Cox, J., Neuhauser, N., Michalski, A., Scheltema, R. A., Olsen, J. V. and Mann, M. (2011). Andromeda: a peptide search engine integrated into the MaxQuant environment. *J. Proteome Res.* **10**, 1794–1805. doi:10.1021/pr101065j
- Cox, J., Hein, M. Y., Lubner, C. A., Paron, I., Nagaraj, N. and Mann, M. (2014). Accurate proteome-wide label-free quantification by delayed normalization and maximal peptide ratio extraction, termed MaxLFQ*. *Mol. Cell. Proteomics* **13**, 2513–2526. doi:10.1074/mcp.M113.031591
- Cullinane, A. R., Schäffer, A. A. and Huizing, M. (2013). The BEACH is hot: a LYST of emerging roles for BEACH-domain containing proteins in human disease. *Traffic* **14**, 749–766. doi:10.1111/tra.12069
- Dawaliby, R. and Mayer, A. (2010). Microautophagy of the nucleus coincides with a vacuolar diffusion barrier at nuclear-vacuolar junctions. *Mol. Biol. Cell* **21**, 4173–4183. doi:10.1091/mbc.e09-09-0782
- Day, K. J., Casler, J. C. and Glick, B. S. (2018). Budding yeast has a minimal endomembrane system. *Dev. Cell* **44**, 56–72.e4. doi:10.1016/j.devcel.2017.12.014
- Dove, S. K., Piper, R. C., McEwen, R. K., Yu, J. W., King, M. C., Hughes, D. C., Thuring, J., Holmes, A. B., Cooke, F. T., Michell, R. H. et al. (2004). Svp1p defines a family of phosphatidylinositol 3,5-bisphosphate effectors. *EMBO J.* **23**, 1922–1933. doi:10.1038/sj.emboj.7600203
- Eising, S., Thiele, L. and Fröhlich, F. (2019). A systematic approach to identify recycling endocytic cargo depending on the GARP complex. *Elife* **8**, e42837. doi:10.7554/eLife.42837
- Faigle, W., Raposo, G., Tenza, D., Pinet, V., Vogt, A. B., Kropshofer, H., Fischer, A., de Saint-Basile, G. and Amigorena, S. (1998). Deficient peptide loading and MHC class II endosomal sorting in a human genetic immunodeficiency disease: the chediak-higashi syndrome. *J. Cell Biol.* **141**, 1121–1134. doi:10.1083/jcb.141.5.1121
- Falkenstein, K. and Lozanne, A. D. (2014). Dictyostelium LvsB has a regulatory role in endosomal vesicle fusion. *J. Cell Sci.* **127**, 4356–4367.
- Ferguson, S. M. (2018). Axonal transport and maturation of lysosomes. *Curr. Opin. Neurobiol.* **51**, 45–51. doi:10.1016/j.conb.2018.02.020
- Fischer, T. D., Wang, C., Padman, B. S., Lazarou, M. and Youle, R. J. (2020). STING induces LC3B lipidation onto single-membrane vesicles via the V-ATPase and ATG16L1-WD40 domain. *J. Cell Biol.* **219**, e202009128. doi:10.1083/jcb.202009128
- Fröhlich, F., Christiano, R. and Walther, T. C. (2013). Native SILAC: metabolic labeling of proteins in prototroph microorganisms based on lysine synthesis regulation. *Mol. Cell. Proteomics* **12**, 1995–2005. doi:10.1074/mcp.M112.025742
- Gomez-Navarro, N. and Miller, E. A. (2016). COP-coated vesicles. *Curr. Biol.* **26**, R54–R57. doi:10.1016/j.cub.2015.12.017
- Guimaraes, R. S., Delorme-Axford, E., Klionsky, D. J. and Reggiori, F. (2015). Assays for the biochemical and ultrastructural measurement of selective and nonselective types of autophagy in the yeast *Saccharomyces cerevisiae*. *Methods* **75**, 141–150. doi:10.1016/j.ymeth.2014.11.023
- Haas, A. (1995). A quantitative assay to measure homotypic vacuole fusion in vitro. *Methods Cell Sci.* **17**, 283–294. doi:10.1007/BF00986234
- Hatakeyama, R., Péli-Gulli, M.-P., Hu, Z., Jaquenoud, M., Osuna, G. M. G., Sardu, A., Dengjel, J. and Virgilio, C. D. (2019). Spatially distinct pools of TORC1 balance protein homeostasis. *Mol. Cell* **73**, 325–338.e8. doi:10.1016/j.molcel.2018.10.040
- Hawkins, W. D. and Klionsky, D. J. (2021). The expanding role of Atg8. *Autophagy* **17**, 3273–3274. doi:10.1080/15548627.2021.1967566
- He, C.-W., Cui, X.-F., Ma, S.-J., Xu, Q., Ran, Y.-P., Chen, W.-Z., Mu, J.-X., Li, H., Zhu, J., Gong, Q. et al. (2021). Membrane recruitment of Atg8 by Hfl1 facilitates turnover of vacuolar membrane proteins in yeast cells approaching stationary phase. *BMC Biol.* **19**, 117. doi:10.1186/s12915-021-01048-7
- Heckmann, B. L. and Green, D. R. (2019). LC3-associated phagocytosis at a glance. *J. Cell Sci.* **132**, jcs222984. doi:10.1242/jcs.222984
- Heckmann, B. L., Teubner, B. J. W., Tummers, B., Boada-Romero, E., Harris, L., Yang, M., Guy, C. S., Zakharenko, S. S. and Green, D. R. (2019). LC3-associated endocytosis facilitates β -amyloid clearance and mitigates neurodegeneration in murine Alzheimer's disease. *Cell* **178**, 536–551.e14. doi:10.1016/j.cell.2019.05.056
- Henne, W. M., Buchkovich, N. J. and Emr, S. D. (2011). The ESCRT pathway. *Dev. Cell* **21**, 77–91. doi:10.1016/j.devcel.2011.05.015
- Herb, M., Gluschko, A. and Schramm, M. (2019). LC3-associated phagocytosis - The highway to hell for phagocytosed microbes. *Semin. Cell Dev. Biol.* **101**, 68–76. doi:10.1016/j.semcdb.2019.04.016

- Holland, P., Torgersen, M. L., Sandvig, K. and Simonsen, A. (2014). LYST affects lysosome size and quantity, but not trafficking or degradation through autophagy or endocytosis. *Traffic* **15**, 1390-1405. doi:10.1111/tra.12227
- Hönscher, C., Mari, M., Auffarth, K., Bohnert, M., Griffith, J., Geerts, W., van der Laan, M., Cabrera, M., Reggiori, F. and Ungermann, C. (2014). Cellular metabolism regulates contact sites between vacuoles and mitochondria. *Dev. Cell* **30**, 86-94. doi:10.1016/j.devcel.2014.06.006
- Horazdovsky, B., Busch, G. and Emr, S. (1994). VPS21 encodes a rab5-like GTP binding protein that is required for the sorting of yeast vacuolar proteins. *EMBO J.* **13**, 1297-1309. doi:10.1002/j.1460-2075.1994.tb06382.x
- Hubner, N. C., Bird, A. W., Cox, J., Spletstoesser, B., Bandilla, P., Poser, I., Hyman, A. and Mann, M. (2010). Quantitative proteomics combined with BAC TransgeneOmics reveals in vivo protein interactions. *J. Cell Biol.* **189**, 739-754. doi:10.1083/jcb.200911091
- Huotari, J. and Helenius, A. (2011). Endosome maturation. *EMBO J.* **30**, 3481-3500. doi:10.1038/emboj.2011.286
- Hutagalung, A. H. and Novick, P. J. (2011). Role of Rab GTPases in membrane traffic and cell physiology. *Physiol. Rev.* **91**, 119-149. doi:10.1152/physrev.00059.2009
- Janke, C., Magiera, M. M., Rathfelder, N., Taxis, C., Reber, S., Maekawa, H., Moreno-Borchart, A., Doenges, G., Schwob, E., Schiebel, E. et al. (2004). A versatile toolbox for PCR-based tagging of yeast genes: new fluorescent proteins, more markers and promoter substitution cassettes. *Yeast (Chichester, England)* **21**, 947-962. doi:10.1002/yea.1142
- Klionsky, D. J., Abdel-Aziz, A. K., Abdelfatah, S., Abdellatif, M., Abdoli, A., Abel, S., Abielovich, H., Abildgaard, M. H., Abudu, Y. P., Acevedo-Arozena, A. et al. (2021). Guidelines for the use and interpretation of assays for monitoring autophagy (4th edition) 1. *Autophagy* **17**, 1-382. doi:10.1080/15548627.2020.1797280
- Langemeyer, L., Borchers, A.-C., Herrmann, E., Füllbrunn, N., Han, Y., Perz, A., Auffarth, K., Kümmel, D. and Ungermann, C. (2020). A conserved and regulated mechanism drives endosomal Rab transition. *Elife* **9**, e56090. doi:10.7554/eLife.56090
- Langemeyer, L., Fröhlich, F. and Ungermann, C. (2018). Rab GTPase function in endosome and lysosome biogenesis. *Trends Cell Biol.* **28**, 957-970. doi:10.1016/j.tcb.2018.06.007
- Legakis, J. E., Yen, W.-L. and Klionsky, D. J. (2007). A cycling protein complex required for selective autophagy. *Autophagy* **3**, 422-432. doi:10.4161/auto.4129
- Leidal, A. M., Huang, H. H., Marsh, T., Solvik, T., Zhang, D., Ye, J., Kai, F., Goldsmith, J., Liu, J. Y., Huang, Y.-H. et al. (2019). The LC3-conjugation machinery specifies the loading of RNA-binding proteins into extracellular vesicles. *Nat. Cell Biol.* **22**, 187-199. doi:10.1038/s41556-019-0450-y
- Liu, X.-M., Yamasaki, A., Du, X.-M., Coffman, V. C., Ohsumi, Y., Nakatogawa, H., Wu, J.-Q., Noda, N. N. and Du, L.-L. (2018). Lipidation-independent vacuolar functions of Atg8 rely on its noncanonical interaction with a vacuole membrane protein. *Elife* **7**, e41237. doi:10.7554/eLife.41237
- Lord, S. J., Velle, K. B., Mullins, R. D. and Fritz-Laylin, L. K. (2020). SuperPlots: communicating reproducibility and variability in cell biology. *J. Cell Biol.* **219**, e202001064. doi:10.1083/jcb.202001064
- Lynch-Day, M. A. and Klionsky, D. J. (2010). The Cvt pathway as a model for selective autophagy. *FEBS Lett.* **584**, 1359-1366. doi:10.1016/j.febslet.2010.02.013
- Lystad, A. H., Carlsson, S. R., de la Ballina, L. R., Kauffman, K. J., Nag, S., Yoshimori, T., Melia, T. J. and Simonsen, A. (2019). Distinct functions of ATG16L1 isoforms in membrane binding and LC3B lipidation in autophagy-related processes. *Nat. Cell Biol.* **21**, 372-383. doi:10.1038/s41556-019-0274-9
- Marshall, R. S., Hua, Z., Mali, S., McLoughlin, F. and Vierstra, R. D. (2019). ATG8-Binding UIM proteins define a new class of autophagy adaptors and receptors. *Cell* **177**, 766-781.e24. doi:10.1016/j.cell.2019.02.009
- Martinez, J. (2018). LAP it up, fuzz ball: a short history of LC3-associated phagocytosis. *Curr. Opin. Immunol.* **55**, 54-61. doi:10.1016/j.coi.2018.09.011
- Maruyama, T., Alam, J. M., Fukuda, T., Kageyama, S., Kirisako, H., Ishii, Y., Shimada, I., Ohsumi, Y., Komatsu, M., Kanki, T. et al. (2021). Membrane perturbation by lipidated Atg8 underlies autophagosome biogenesis. *Nat. Struct. Mol. Biol.* **28**, 583-593. doi:10.1038/s41594-021-00614-5
- Mizushima, N. (2020). The ATG conjugation systems in autophagy. *Curr. Opin. Cell Biol.* **63**, 1-10. doi:10.1016/j.cob.2019.12.001
- Munn, A. L. and Riezman, H. (1994). Endocytosis is required for the growth of vacuolar H(+)-ATPase-defective yeast: identification of six new END genes. *J. Cell Biol.* **127**, 373-386. doi:10.1083/jcb.127.2.373
- Nakatogawa, H. (2020). Mechanisms governing autophagosome biogenesis. *Nat. Rev. Mol. Cell Bio.* **21**, 439-458. doi:10.1038/s41580-020-0241-0
- Nickerson, D. P., Russell, M. R. G., Lo, S.-Y., Chapin, H. C., Milnes, J. M. and Merz, A. J. (2012). Termination of isoform-selective Vps21/Rab5 signaling at endolysosomal organelles by Msb3/Gyp3. *Traffic (Copenhagen, Denmark)* **13**, 1411-1428. doi:10.1111/j.1600-0854.2012.01390.x
- Oku, M., Maeda, Y., Kagohashi, Y., Kondo, T., Yamada, M., Fujimoto, T. and Sakai, Y. (2017). Evidence for ESCRT- and clathrin-dependent microautophagy. *J. Cell Biol.* **216**, 3263-3274. doi:10.1083/jcb.201611029
- Olsen, J. V., Macek, B., Lange, O., Makarov, A., Horning, S. and Mann, M. (2007). Higher-energy C-trap dissociation for peptide modification analysis. *Nat. Methods* **4**, 709-712. doi:10.1038/nmeth1060
- Ostrowicz, C. W., Bröcker, C., Ahnert, F., Nordmann, M., Lachmann, J., Peplowska, K., Perz, A., Auffarth, K., Engelbrecht-Vandré, S. and Ungermann, C. (2010). Defined subunit arrangement and rab interactions are required for functionality of the HOPS tethering complex. *Traffic* **11**, 1334-1346. doi:10.1111/j.1600-0854.2010.01097.x
- Paulsel, A. L., Merz, A. J. and Nickerson, D. P. (2013). Vps9 family protein Muk1 is the second Rab5 guanosine nucleotide exchange factor in budding yeast. *J. Biol. Chem.* **288**, 18162-18171. doi:10.1074/jbc.M113.457069
- Perou, C. M., Leslie, J. D., Green, W., Li, L., Ward, D. M. and Kaplan, J. (1997). The beige/chediak-higashi syndrome gene encodes a widely expressed cytosolic protein. *J. Biol. Chem.* **272**, 29790-29794. doi:10.1074/jbc.272.47.29790
- Peter, A. T. J., Lachmann, J., Rana, M., Bunge, M., Cabrera, M. and Ungermann, C. (2013). The BLOC-1 complex promotes endosomal maturation by recruiting the Rab5 GTPase-activating protein Msb3. *J. Cell Biol.* **201**, 97-111. doi:10.1083/jcb.201210038
- Preston, R. A., Reinagel, P. S. and Jones, E. W. (1992). Genes required for vacuolar acidity in *Saccharomyces cerevisiae*. *Genetics* **131**, 551-558. doi:10.1093/genetics/131.3.551
- Rahman, M., Haberman, A., Tracy, C., Ray, S. and Krämer, H. (2012). *Drosophila* mauve mutants reveal a role of LYST homologs late in the maturation of phagosomes and autophagosomes. *Traffic* **13**, 1680-1692. doi:10.1111/tra.12005
- Rains, A., Bryant, Y., Dorsett, K. A., Culver, A., Egbaria, J., Williams, A., Barnes, M., Lamere, R., Rossi, A. R., Waldrep, S. C. et al. (2017). Ypt4 and Ivs1 regulate vacuolar size and function in *Schizosaccharomyces pombe*. *Cell Logist* **7**, e1335270. doi:10.1080/21592799.2017.1335270
- Raymond, C., Howald-Stevenson, I., Vater, C. and Stevens, T. (1992). Morphological classification of the yeast vacuolar protein sorting mutants: evidence for a prevacuolar compartment in class E vps mutants. *Mol. Biol. Cell* **3**, 1389-1402. doi:10.1091/mbc.3.12.1389
- Reggiori, F. and Ungermann, C. (2017). Autophagosome maturation and fusion. *J. Mol. Biol.* **429**, 486-496. doi:10.1016/j.jmb.2017.01.002
- Robinson, J., Klionsky, D., Banta, L. and Emr, S. (1988). Protein sorting in *Saccharomyces cerevisiae*: isolation of mutants defective in the delivery and processing of multiple vacuolar hydrolases. *Mol. Cell. Biol.* **8**, 4936-4948.
- Rothman, J. H. and Stevens, T. H. (1986). Protein sorting in yeast: Mutants defective in vacuole biogenesis mislocalize vacuolar proteins into the late secretory pathway. *Cell* **47**, 1041-1051. doi:10.1016/0092-8674(86)90819-6
- Sánchez-Wandelmer, J., Kriegenburg, F., Rohringer, S., Schuschnig, M., Gómez-Sánchez, R., Zens, B., Abreu, S., Hardenberg, R., Hollenstein, D., Gao, J. et al. (2017). Atg4 proteolytic activity can be inhibited by Atg1 phosphorylation. *Nat. Commun.* **8**, 295. doi:10.1038/s41467-017-00302-3
- Saxton, R. A. and Sabatini, D. M. (2017). mTOR signaling in growth, metabolism, and disease. *Cell* **168**, 960-976. doi:10.1016/j.cell.2017.02.004
- Schäfer, J. A., Schessner, J. P., Bircham, P. W., Tsuji, T., Funaya, C., Pajonk, O., Schaeff, K., Ruffini, G., Papagiannidis, D., Knop, M. et al. (2019). ESCRT machinery mediates selective microautophagy of endoplasmic reticulum in yeast. *EMBO J.* **39**, e102586.
- Schoppe, J., Mari, M., Yavavli, E., Auffarth, K., Cabrera, M., Walter, S., Fröhlich, F. and Ungermann, C. (2020). AP-3 vesicle uncoating occurs after HOPS-dependent vacuole tethering. *EMBO J.* **39**, e2020105117. doi:10.15252/emboj.2020105117
- Schuck, S. (2020). Microautophagy – distinct molecular mechanisms handle cargoes of many sizes. *J. Cell Sci.* **133**, jcs246322. doi:10.1242/jcs.246322
- Sepulveda, F. E., Burgess, A., Heiligenstein, X., Goudin, N., Ménager, M. M., Romao, M., Côte, M., Mahlaoui, N., Fischer, A., Raposo, G. et al. (2015). LYST Controls the biogenesis of the endosomal compartment required for secretory lysosome function. *Traffic* **16**, 191-203. doi:10.1111/tra.12244
- Sharma, P., Nicoli, E.-R., Serra-Vinardell, J., Morimoto, M., Toro, C., Malicdan, M. C. V. and Introne, W. J. (2019). Chediak-Higashi syndrome: a review of the past, present, and future. *Drug Discov. Today Dis. Model.* **31**, 31-36. doi:10.1016/j.ddmod.2019.10.008
- Shiflett, S. L., Vaughn, M. B., Huynh, D., Kaplan, J. and Ward, D. M. (2004). Bph1p, the *Saccharomyces cerevisiae* Homologue of CHS1/Beige, functions in cell wall formation and protein sorting. *Traffic (Copenhagen, Denmark)* **5**, 700-710. doi:10.1111/j.1600-0854.2004.00213.x
- Shin, H. R. and Zoncu, R. (2020). The lysosome at the intersection of cellular growth and destruction. *Dev. Cell* **54**, 226-238. doi:10.1016/j.devcel.2020.06.010

- Singer-Krüger, B., Stenmark, H., Düsterhöft, A., Philippsen, P., Yoo, J. S., Gallwitz, D. and Zerial, M.** (1994). Role of three rab5-like GTPases, Ypt51p, Ypt52p, and Ypt53p, in the endocytic and vacuolar protein sorting pathways of yeast. *J. Cell Biol.* **125**, 283-298. doi:10.1083/jcb.125.2.283
- Teh, O., Hatsugai, N., Tamura, K., Fuji, K., Tabata, R., Yamaguchi, K., Shingenobu, S., Yamada, M., Hasebe, M., Sawa, S. et al.** (2015). BEACH-domain proteins act together in a cascade to mediate vacuolar protein trafficking and disease resistance in arabidopsis. *Mol. Plant* **8**, 389-398. doi:10.1016/j.molp.2014.11.015
- Vida, T. A. and Emr, S. D.** (1995). A new vital stain for visualizing vacuolar membrane dynamics and endocytosis in yeast. *J. Cell Biol.* **128**, 779-792. doi:10.1083/jcb.128.5.779
- Virgilio, C. D.** (2012). The essence of yeast quiescence. *FEMS Microbiol. Rev.* **36**, 306-339. doi:10.1111/j.1574-6976.2011.00287.x
- Wada, Y., Ohsumi, Y. and Anraku, Y.** (1992). Genes for directing vacuolar morphogenesis in *Saccharomyces cerevisiae*. I. Isolation and characterization of two classes of vam mutants. *J. Biol. Chem.* **267**, 18665-18670.
- Wandinger-Ness, A. and Zerial, M.** (2014). Rab proteins and the compartmentalization of the endosomal system. *Cold Spring Harbor Perspect. Biol.* **6**, a022616. doi:10.1101/cshperspect.a022616
- Wichmann, H., Hengst, L. and Gallwitz, D.** (1992). Endocytosis in yeast: evidence for the involvement of a small GTP-binding protein (Ypt7p). *Cell* **71**, 1131-1142. doi:10.1016/S0092-8674(05)80062-5
- Wilfling, F., Lee, C.-W., Erdmann, P. S., Zheng, Y., Sherpa, D., Jentsch, S., Pfander, B., Schulman, B. A. and Baumeister, W.** (2020). A selective autophagy pathway for phase-separated endocytic protein deposits. *Mol. Cell* **80**, 764-778.e7. doi:10.1016/j.molcel.2020.10.030
- Zellner, S., Schifferer, M. and Behrends, C.** (2021). Systematically defining selective autophagy receptor-specific cargo using autophagosome content profiling. *Mol. Cell* **81**, 1337-1354.e8. doi:10.1016/j.molcel.2021.01.009
- Zhao, Y. G. and Zhang, H.** (2018). Autophagosome maturation: an epic journey from the ER to lysosomes. *J. Cell Biol.* **218**, 757-770. doi:10.1083/jcb.201810099